

Supporting Information for:

A Triply Linked Propellane–Nanoring Hybrid Serving as Good Host

Yan Chen,^{[a]‡} Xingyu Chen,^{[b]‡} Lin Li,^{[c]‡} Xiangping Chen,^{[a]‡} Jianlong Xia,^[b] and Lei Zhang^{*[a]}

^[a] Beijing Advanced Innovation Center for Soft Matter Science and Engineering, State Key Lab of Organic-Inorganic Composites, College of Materials Science and Engineering, Beijing University of Chemical Technology, Beijing 100029 (P. R. China)

^[b] State Key Laboratory of Advanced Technology for Materials Synthesis and Processing, Center of Smart Materials and Devices, Wuhan University of Technology, Wuhan 430070 (P. R. China)

^[c] Key Laboratory of the Ministry of Education for Advanced Catalysis Materials, College of Chemistry and Materials Science, Zhejiang Normal University, Jinhua 321004, P.R. China

^[‡] These authors contributed equally to this work.

Table of Contents

1. Materials and Methods.....	S2
2. Synthesis and Characterization of Compounds.....	S2
3. X-ray Crystallographic Data for Compounds.....	S3
4. Binding Behaviors with C ₆₀	S6
5. Density Functional Theory Results.....	S8
6. UV, CV and PL Spectra of Compounds.....	S11
7. Transient Absorption Measurements.....	S11
8. Adsorption Isotherms Tests.....	S14
9. Breakthrough Curves Tests.....	S16
10. IAST (Ideal adsorbed solution theory) Selectivity Calculations.....	S16
11. Isothermic Heats of Adsorption (Q _{st}) Calculations.....	S17
12. Binding Energy Calculations.....	S18
13. ¹ H NMR, ¹³ C NMR, and HRMS Spectra of Compounds.....	S19
14. References.....	S26

Experimental Procedures

1. Materials and Methods

All chemicals were purchased from commercial suppliers and used without further purification unless otherwise specified. Toluene were freshly distilled over sodium prior to use. ^1H NMR and ^{13}C NMR spectra were recorded in deuterated solvents on Bruker ADVANCE 400 NMR Spectrometer. ^1H NMR spectra were referenced to the signals of CDCl_3 ($\delta = 7.26$ ppm) or $\text{C}_2\text{D}_2\text{Cl}_4$ ($\delta = 6.00$ ppm). ^{13}C NMR spectra were referenced to the signals of CDCl_3 ($\delta = 77.20$ ppm). High resolution mass spectra (HRMS) were determined on IonSpec 9.4 Tesla Fourier Transform Mass Spectrometer.

2. Synthesis and Characterization of Compounds

Synthesis of *m*-terphenyl borate 2

To a 100 ml two-neck round bottomed flask was added *m*-terphenyl bromide ^[1](1 g, 2.05 mmol), bis(pinacolato)diboron (0.78 g, 3.08 mmol), $\text{PdCl}_2(\text{dppf})$ (0.075 g, 0.1 mmol), Potassium acetate (0.6 g, 6.15 mmol) in anhydrous DMSO (25 ml), The mixture was stirred under nitrogen and heated at 110 °C for 8 hours. After cooling, the mixture was extracted with dichloromethane, washed with water and dried over anhydrous sodium sulfate. The solvent was evaporated in vacuo and the crude material was purified by silica gel column chromatography (petroleum ether: dichloromethane = 3:1) to afford compound 2 as a white solid (0.82 g, yields: 75 %). ^1H NMR (400 MHz, Chloroform-*d*) δ 7.96 (d, $J = 1.8$ Hz, 2H), 7.75 (t, $J = 1.9$ Hz, 1H), 7.49 (t, $J = 1.6$ Hz, 2H), 7.45 (t, $J = 1.7$ Hz, 2H), 7.36 (t, $J = 1.8$ Hz, 2H), 1.39 (s, 12H), 1.37 (s, 18H). ^{13}C NMR (101 MHz, Chloroform-*d*) δ 153.79, 142.73, 140.85, 134.48, 133.09, 129.32, 124.88, 123.01, 84.28, 35.22, 31.44, 25.03. HR-EI (m/z): calcd. for $\text{C}_{32}\text{H}_{30}\text{BCl}_2\text{O}_2$ 536.242, found 536.241.

Synthesis of compound 3

To a sealed tube was added with TPPTI-Br₆ (100 mg, 0.052 mmol), *m*-terphenyl borate 2 (123 mg, 0.23 mmol), $\text{Pd}(\text{PPh}_3)_4$ (8 mg, 0.007 mmol), 2 M aq. K_2CO_3 (7 ml), and THF (14 ml), the mixture was stirred under nitrogen and then refluxed overnight. After cooling, the organic layer was separated and removed in vacuo, the crude product was purified by silica gel column chromatography (petroleum ether: dichloromethane = 3:1) to afford compound 3 as a red solid (160 mg, yields: 80 %). ^1H NMR (400 MHz, Chloroform-*d*) δ 8.56 (d, $J = 13.1$ Hz, 6H), 7.73 (d, $J = 8.0$ Hz, 6H), 7.64 (s, 6H), 7.48 (s, 12H), 7.44 (d, $J = 8.0$ Hz, 6H), 7.32 (s, 12H), 7.21 (s, 24H), 5.25-5.17 (m, 3H), 2.31-2.22 (m, 6H), 1.88-1.82 (m, 6H), 1.36-1.24 (m, 48H), 1.15 (s, 96H), 0.83 (t, $J = 6.8$ Hz, 18H). ^{13}C NMR (101 MHz, Chloroform-*d*) δ 153.38, 145.72, 144.82, 142.98, 141.69, 138.09, 136.57, 134.58, 134.27, 132.68, 130.39, 129.89, 128.37, 127.63, 126.74, 125.54, 125.09, 124.80, 122.37, 119.25, 80.27, 54.38, 34.66, 32.41, 32.02, 31.00, 29.98, 26.82, 22.96, 14.32. HR-MALDI-TOF (m/z): calcd. for $\text{C}_{257}\text{H}_{249}\text{Cl}_{12}\text{N}_3\text{O}_6$ 3900.553, found 3900.551.

Synthesis of TPPTI-[9]CMP

Bis(1,5-cyclooctadiene)nickel(0) (2 g, 7.3 mmol) was added to the mixture of 2,2'-bipyridine (0.79 g, 7.3 mmol), 1,5-cyclooctadiene (1.1 g, 7.3 mmol) in anhydrous toluene (15 ml) and DMF (15 ml) under nitrogen, and then stirred at 80 °C for 30 min. A solution of compound 3 (120 mg, 0.031 mmol) in anhydrous toluene (5 ml) and DMF (25 mL) was added dropwise over 30 min. The mixture was stirred and heated at 80 °C for 8 h. After cooling, the solvent was evaporated in vacuo and the crude product was purified by silica gel column chromatography (petroleum ether: dichloromethane = 5:1) to afford TPPTI-[9]CMP as a red solid (54 mg, yields: 50 %). ¹H NMR (400 MHz, 1,1,2,2-Tetrachloroethane-*d*₂) δ 8.65 (d, J = 12.0 Hz, 6H), 7.77 (s, 6H), 7.51 (s, 12H), 7.48 (s, 12H), 7.34 (s, 12H), 7.28-7.25 (m, 18H), 7.04 (d, J = 8.0 Hz, 6H), 5.20-5.08 (m, 3H), 2.23-2.18 (m, 6H), 1.88-1.85(m, 6H), 1.38 (s, 96H), 1.26 (s, 48H), 0.87-0.85 (m, 18H). ¹³C NMR (101 MHz, Chloroform-*d*) δ 164.73 , 163.83 , 151.68 , 146.40 , 144.86 , 143.40 , 142.18 , 138.27 , 135.98 , 135.14 , 134.30 , 133.57 , 131.58 , 129.91 , 129.49 , 128.87 , 128.81 , 127.87 , 126.81 , 125.60 , 124.96 , 124.32 , 119.66 , 54.52 , 34.98 , 32.52 , 32.18 , 31.59 , 30.10 , 26.91 , 23.11 , 14.44 . HR-MALDI-TOF (m/z): calcd. for C₂₅₇H₂₄₉N₃O₆ 3474.934, found 3474.931.

Synthesis of [9]CMP

Compound 4 was prepared according to the reported procedure.^[2] Bis(1,5-cyclooctadiene)nickel(0) (497.5 mg, 1.809 mmol) was added to the mixture of 2,2'-bipyridine (282.2 mg, 1.809 mmol), 1,5-cyclooctadiene (195.4 mg, 1.809 mmol) in anhydrous toluene (20 ml) and DMF (7 ml,) under nitrogen, and then stirred at 80 °C for 30 min. A solution of compound 4 (200 mg, 0.402 mmol) in anhydrous toluene (15 mL) was added dropwise over 30 min. The mixture was stirred and heated at 80 °C for 16 h. After cooling, the solvent was evaporated in vacuo and the crude product was purified by silica gel column chromatography (petroleum ether: dichloromethane = 12:1) to afford [9]CMP as a white solid (4 mg , yields: 3 %). ¹H NMR (400 MHz, Chloroform-*d*) δ 7.78 (s, 3H), 7.59-7.58 (m, 24H), 7.53-7.50 (m, 3H), 1.41 (s, 54H). ¹³C NMR (101 MHz, Chloroform-*d*) δ 152.20, 142.70, 142.54, 141.89, 129.17, 127.35, 126.57, 124.48, 123.99, 123.89, 35.14, 31.66, 27.08. HR-MALDI-TOF (m/z): calcd. for C₇₈H₈₄ 1020.657, found 1020.658.

3. X-ray Crystallographic Data for Compounds

Single crystals of TPPTI-[9]CMP, (C₆₀)₃@TPPTI-[9]CMP and [9]CMP suitable for X-ray diffraction analysis were grown by slow diffusion of methanol into CHCl₃ and toluene solution at room temperature. The X-ray diffraction data were collected on a MM007HF Saturn724+ diffractometer with graphite monochromated Cu Kα (1.54184 Å). Since the crystals of TPPTI-[9]CMP and (C₆₀)₃@TPPTI-[9]CMP obtained were either very small or lost solvent rapidly, the collect data are of relatively low quality but the overall connectivity of the structures can be unambiguously determined. It was necessary to use PLATON-SQUEEZE^[3] in all refinements: generally the number of electrons, and amount of solvent, accounted for by the SQUEEZE routine is significantly higher than the amount of solvent indicated by TGA. This is unsurprising as the solvent loss that may also occur during sample preparation for TGA measurement.

TPPTI-[9]CMP: The structure contained some diffuse electron density which appeared to correspond to disordered chloroform. As these could not be sensibly modelled, the data was processed with PLATON-SQUEEZE to account for the residual electron density (estimated total void volume: 6749 Å³, estimated total electron count: 1802). The majority of the alkyl chains and t-Bu groups were modelled with DFIX restraints to give a chemically-sensible model.

(C₆₀)₃@TPPTI-[9]CMP: The structure contained some diffuse electron density which appeared to correspond to disordered methanol and toluene. As these could not be sensibly modelled, the data was processed with PLATON-

SQUEEZE to account for the residual electron density (estimated total void volume: 5672 Å³, estimated total electron count: 1421). The majority of the alkyl chains, t-Bu groups, and disordered C₆₀ were modelled with DFIX restraints to give a chemically-sensible model.

Crystallographic data have been deposited with the Cambridge Crystallographic Data Centre as supplementary publication No. CCDC 2416457 (TPPTI-[9]CMP), 2416458 ((C₆₀)₃@TPPTI-[9]CMP) and 2416459 ([9]CMP). The single crystal X-ray crystallographic data were summarized in Table S1.

Table S1. Crystal data and structure refinement for TPPTI-[9]CMP, (C₆₀)₃@TPPTI-[9]CMP and [9]CMP.

Identification code	TPPTI-[9]CMP	[9]CMP	(C ₆₀) ₃ @TPPTI-[9]CMP
Empirical formula	C ₂₇₂ Cl ₄₅ H ₂₆₄ N ₃ O ₆	C ₈₂ H ₈₈ Cl ₁₂	C ₅₂₈ H ₃₅₃ N ₃ O ₆
Formula weight	5266.10	1498.92	6835.11
Crystal system	Triclinic	Monoclinic	Triclinic
Space group	P-1	C2/c	P-1
Radiation type	Cu Kα	Cu Kα	Cu Kα
Radiation wavelength(Å)	1.54178	1.54184	1.54178
T(K)	100(1)	170.00(10)	170(1)
a(Å)	21.8575(8)	16.4184(2)	22.4394(11)
b(Å)	27.0119(7)	29.5605(4)	25.0320(12)
c(Å)	27.2218(8)	16.8961(2)	34.7003(12)
α(deg)	78.849(2)	90	84.936(3)
β(deg)	76.570(3)	101.8490(10)	79.688(4)
γ(deg)	80.260(3)	90	67.852(5)
V(Å ³)	15206.9(9)	8025.56(18)	17756.9(15)
Z	2	4	2
ρ _{calc} (g cm ⁻³)	1.150	1.241	1.278
θ, range(°)	2.405 to 66.05	2.99 to 76.152	2.589 to 66.049
μ(mm ⁻¹)	4.048	4.102	0.564
F(000)	3720	3136.0	7180
Crystal size (mm ³)	0.100x0.040x0.030	0.23x0.04x0.03	0.11x0.08x0.05
Index ranges	-25 ≤ h ≤ 25, -32 ≤ k ≤ 31, -32 ≤ l ≤ 30	-20 ≤ h ≤ 20, -36 ≤ k ≤ 26, -21 ≤ l ≤ 21	-26 ≤ h ≤ 26, -27 ≤ k ≤ 29, -41 ≤ l ≤ 41
Reflections collected	167629	29421	219520
Independent reflections	52580 [R _{int} = 0.1005]	8051 [R _{int} = 0.0330, R _{sigma} = 0.0310]	61475 [R _{int} = 0.129]
Data / restraints / parameters	52580/971/2239	8051/156/506	61475/10784/3320
Goodness-of-fit on F ²	1.097	1.039	1.029
Final R indices [I>2σ(I)]	R ₁ = 0.0840, wR ₂ = 0.1935	R ₁ = 0.0813, wR ₂ = 0.2260	R ₁ = 0.1478, wR ₂ = 0.2824
R indices(all data)	R ₁ = 0.1357, wR ₂ = 0.2053	R ₁ = 0.0920, wR ₂ = 0.2358	R ₁ = 0.2463, wR ₂ = 0.3106
Largest diff. peak and hole(e.Å ⁻³)	0.407/-0.289	1.19/-0.62	0.622/-0.379

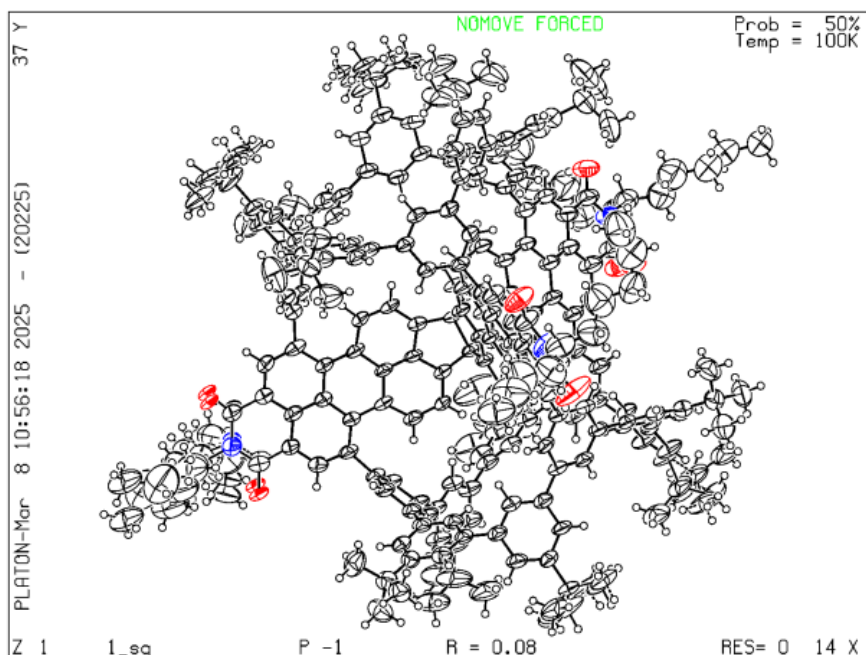


Fig. S1 Thermal ellipsoids drawn at the 50% probability level of TPPTI-[9]CMP. Nitrogen atoms are depicted by blue ellipsoids; Oxygen atoms are depicted by red ellipsoids; Hydrogens are depicted by white circles.

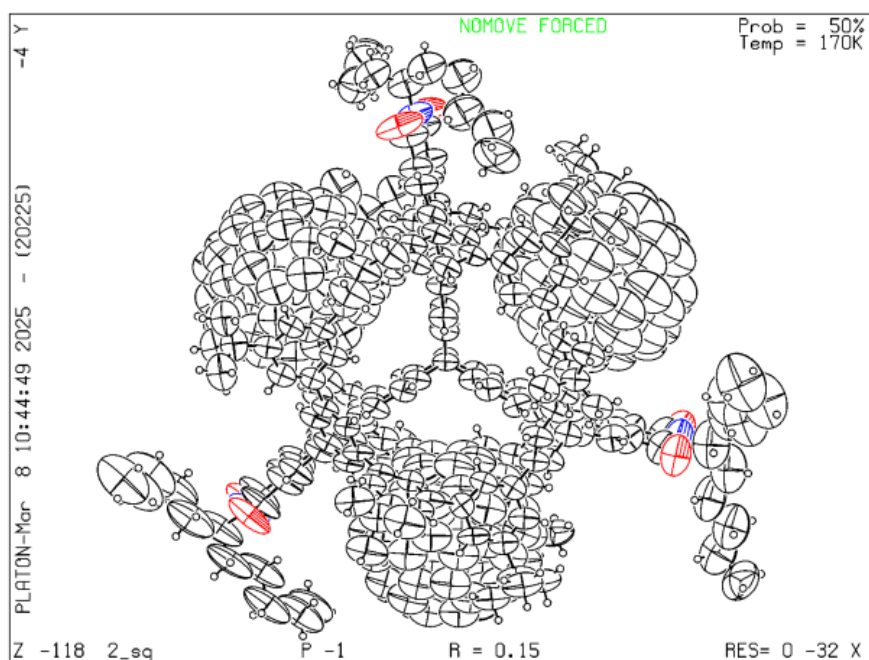


Fig. S2 Thermal ellipsoids drawn at the 50% probability level of (C₆₀)₃@TPPTI-[9]CMP. Nitrogen atoms are depicted by blue ellipsoids; Oxygen atoms are depicted by red ellipsoids; Hydrogens are depicted by white circles.

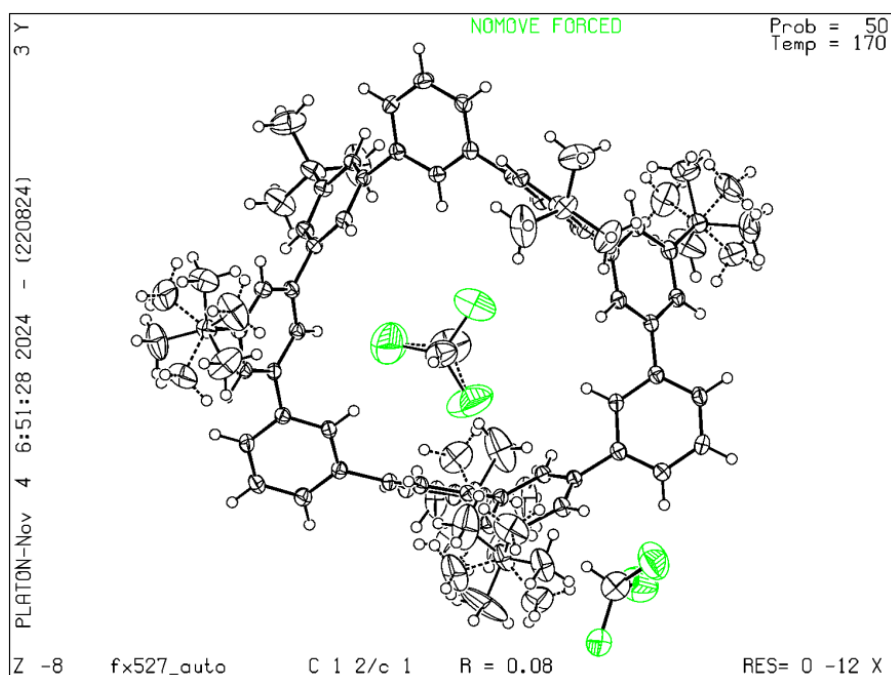


Fig. S3 Thermal ellipsoids drawn at the 50% probability level of [9]CMP. Chlorine atoms are depicted by green ellipsoids; Hydrogens are depicted by white circles.

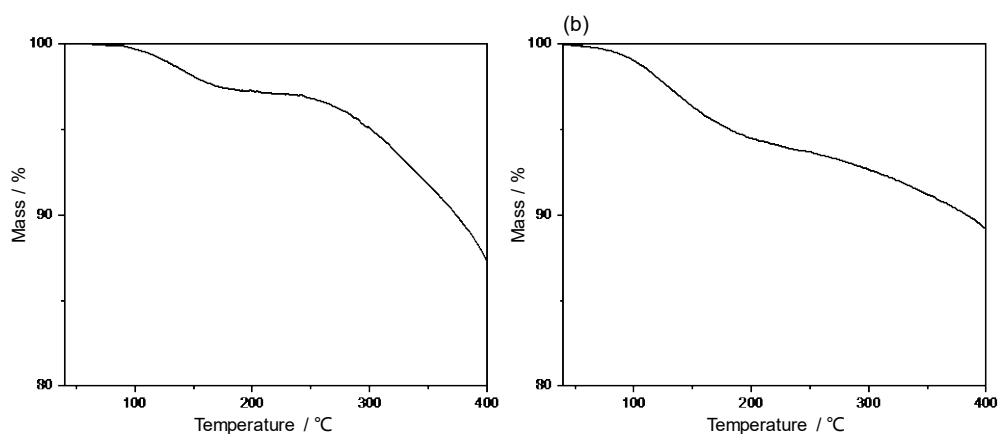


Fig. S4 Thermogravimetric analysis (TGA) of TPPTI-[9]CMP (a) and $(C_{60})_3@TPPTI-[9]CMP$ (b). (Samples were heated at $10.0\text{ }^\circ\text{C}/\text{min}$ from 40 to $400\text{ }^\circ\text{C}$ under a nitrogen flow rate of $50\text{ mL}/\text{min}$. All experiments used $3.0\text{--}5.0\text{ mg}$ of as-grown materials)

4. Binding Behaviors with C_{60}

For Job's plot. A solution of TPPTI-[9]CMP in toluene ($2.0 \times 10^{-6}\text{ M}$) and a solution of C_{60} in toluene ($2.0 \times 10^{-6}\text{ M}$) were mixed in different ratios (TPPTI-[9]CMP: C_{60} = 10:0, 9:1, 8:2, 7:3, 2:1, 6:4, 5:5, 4:6, 1:2, 3:7, 2:8, 1:9, 0:10). The fluorescence emission was measured for each sample, and the differences in the emission at 584 nm were monitored; The Job's plot of TPPTI-[9]CMP and C_{60} in toluene at room temperature.

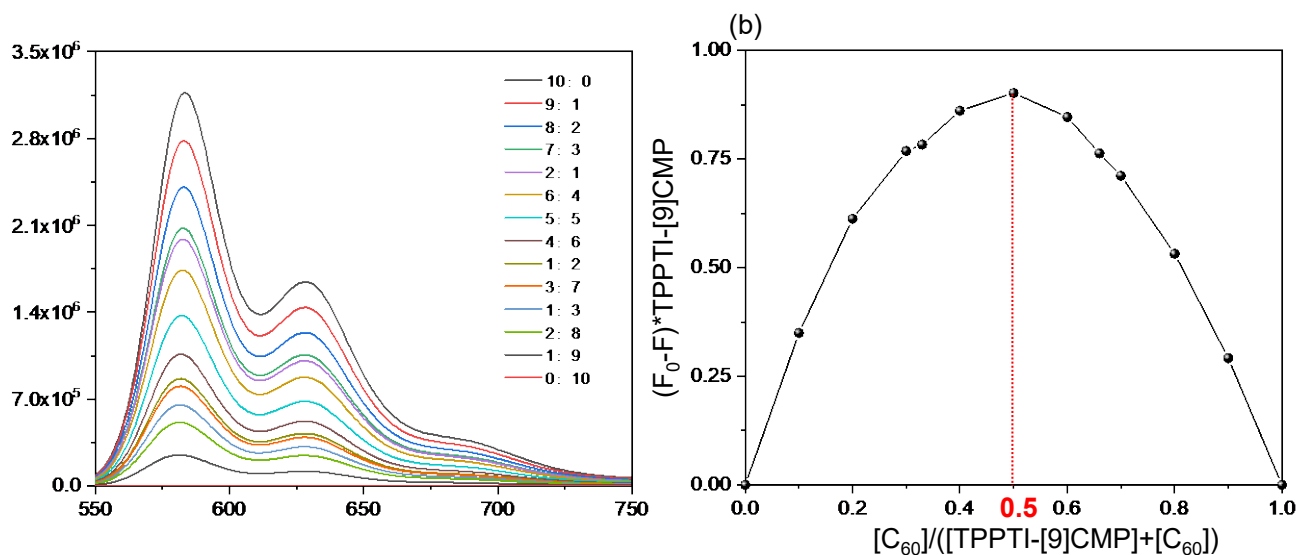


Fig. S5 Fluorescence emission spectra and the Job's plot of TPPTI-[9]CMP and C₆₀ in toluene.

Fluorescence titration experiment by the addition of C₆₀ (10^{-5} M) to TPPTI-[9]CMP (10^{-6} M) in toluene. The changes in the fluorescent intensity of TPPTI-[9]CMP at 584 nm was measured. The K_a was determined by using eq S1.

$$F/F_0 = (1 + K_a [C_{60}]) / (1 + K_a [C_{60}]) \quad (\text{S1})$$

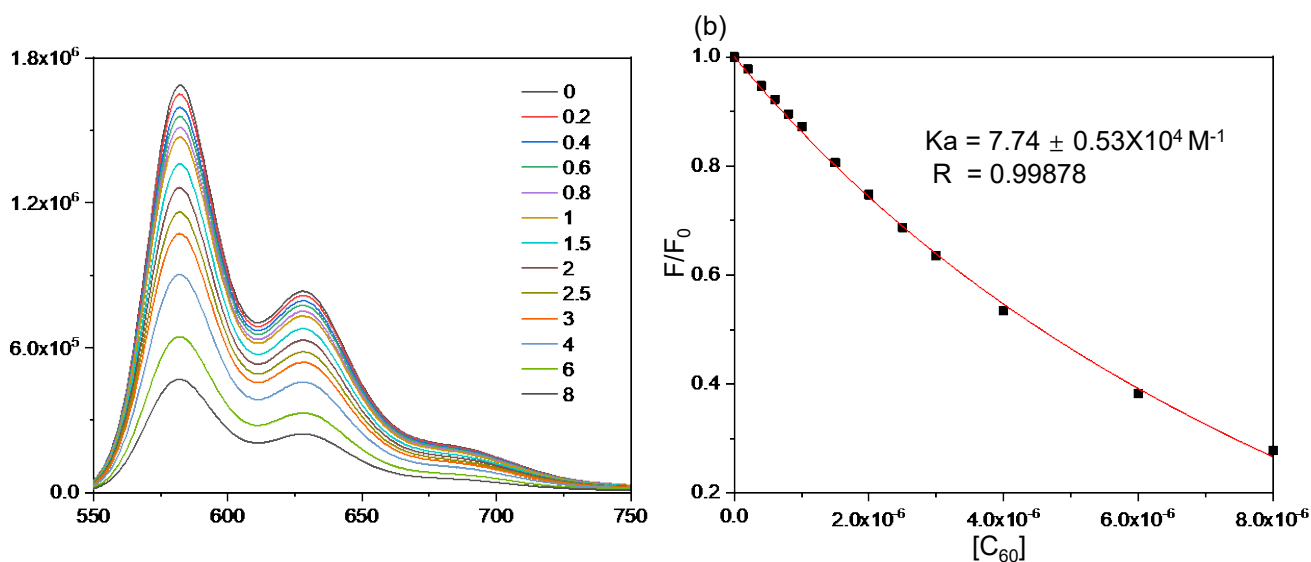


Fig. S6 Fluorescence spectrum of TPPTI-[9]CMP (1.0×10^{-5} M) in the presence of C₆₀ in toluene (a) and correlation of [C₆₀] on the fluorescent intensity of TPPTI-[9]CMP in toluene for obtaining the K_a. R is the coefficient of determination (b).

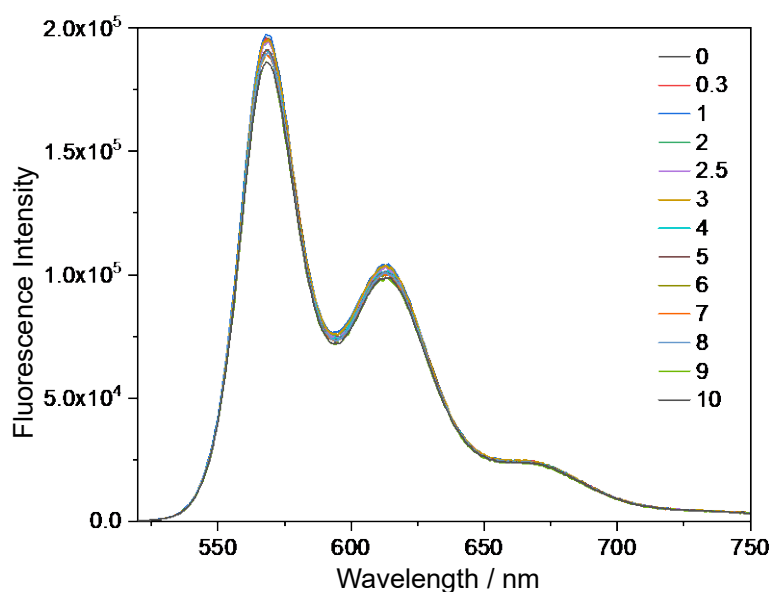


Fig. S7 Fluorescence spectrum of TPPTI (1.0×10^{-5} M) in the presence of C_{60} in toluene.

5. Density Functional Theory Results

All density functional theory (DFT) calculations were performed using Gaussian 09, Revision D.01 program.^[4] All optimized structures were conducted at the B₃LYP level with the 6-31G(d) basis set at gas phase. Time-dependent density functional theory (TD-DFT) were calculated at the B₃LYP/6-31G(d) level in CHCl₃ with the IEFPCM solvent model and at least the 100 excited states were considered. For better comparison with experimental data, Lorentz broadening with a half width at half height of 0.3 eV was applied to the line spectra obtained. Major orbital transition contributions in excited states were generated using Multiwfn 3.8 software.^[5] The cocrystals were used to calculate the weak interactions. To visualize the intermolecular interactions in (C₆₀)₃@TPPTI-[9]CMP, the independent gradient model based on the Hirshfeld partition of molecular density (IGMH) method was conducted by Multiwfn 3.8 software.^[6] The isosurface maps were conducted by VMD.^[7] All details for running StrainViz can be found at <https://github.com/CurtisColwell/StrainViz>.^[8]

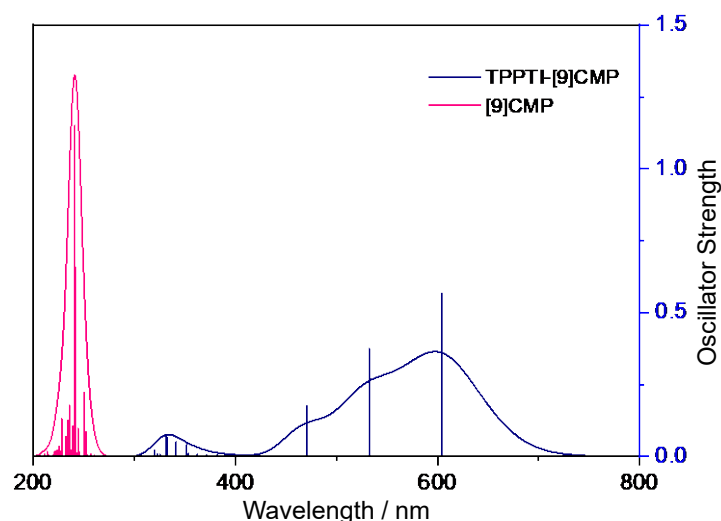


Fig. S8 Computational absorption spectra of TPPTI-[9]CMP and [9]CMP at the B₃LYP/6-31G(d) level in CHCl₃ solution.

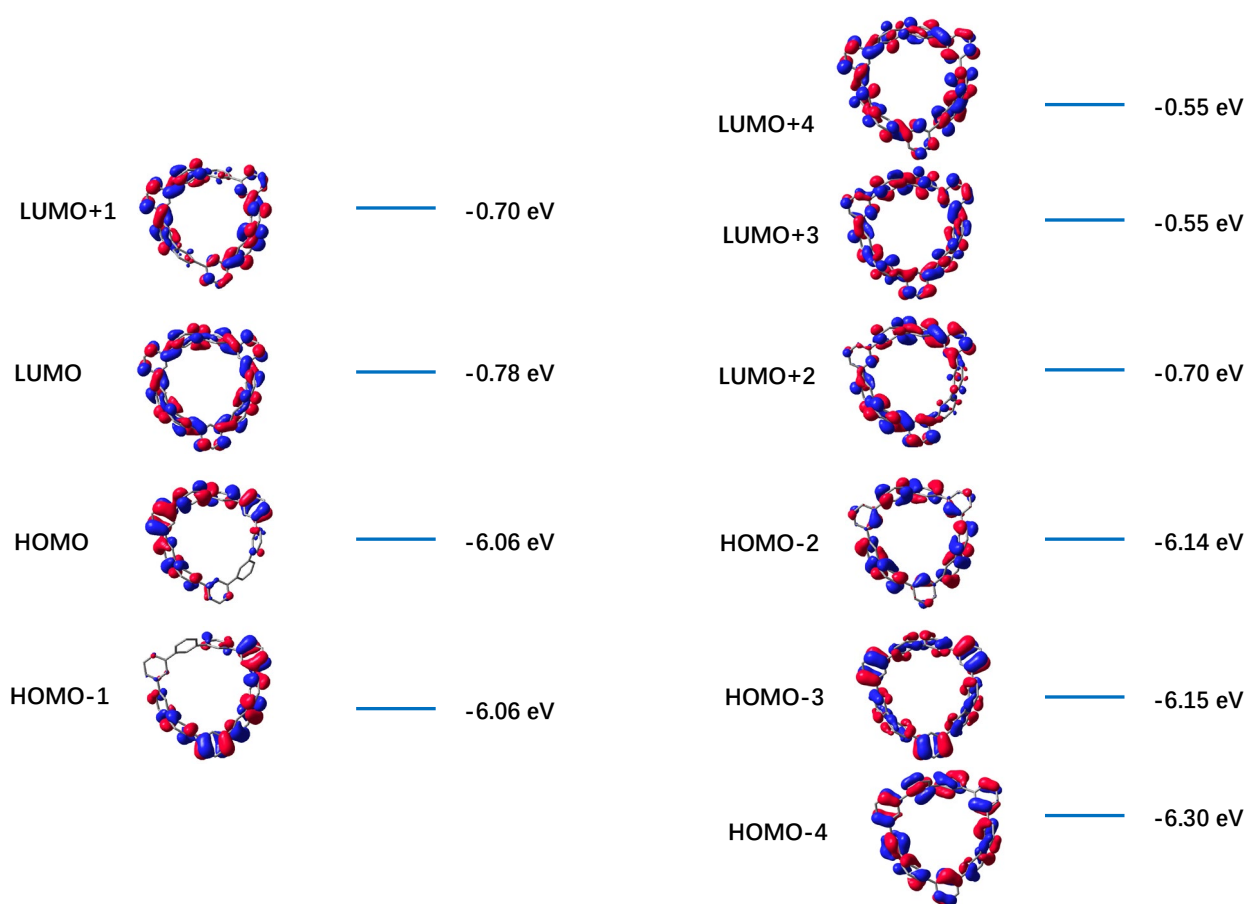


Fig. S9 Pictorial representations of selected frontier molecular orbitals of [9]CMP as determined at the B₃LYP/6-31g(d) level of theory.

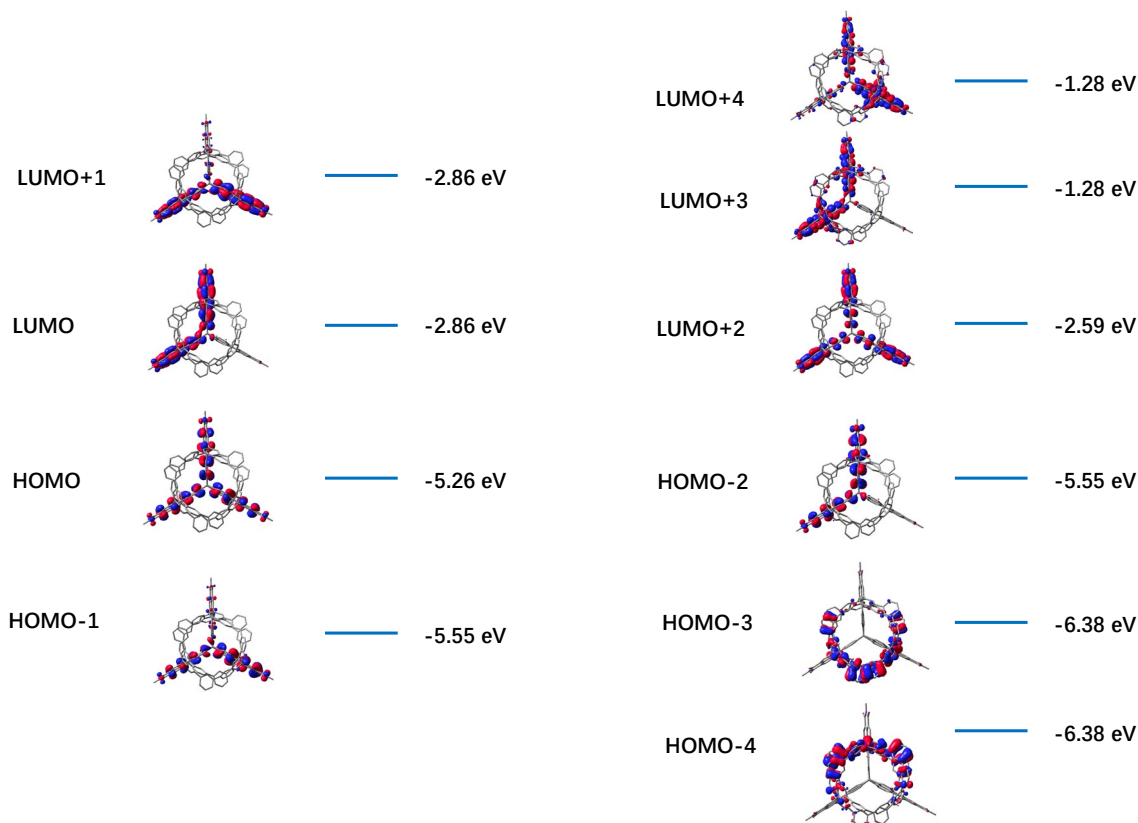


Fig. S10 Pictorial representations of selected frontier molecular orbitals of TPPTI-[9]CMP as determined at the B₃LYP/6-31g(d) level of theory.

Table S2. TD-DFT singlet excitation energies E , excitation wavelengths λ , oscillator strengths f , and orbital contributions of TPPTI-[9]CMP and [9]CMP the B₃LYP/6-31G(d) level in CHCl₃ solution.

	Transition	Energy (eV)	Wavelength (nm)	f	Electronic Configuration
TPPTI-[9]CMP	S ₀ → S ₁	2.0516	604.33	0.56500	HOMO → LUMO (99.1%)
	S ₀ → S ₂	2.0518	604.27	0.56640	HOMO → LUMO+1 (99.1%)
	S ₀ → S ₄	2.3277	532.65	0.17830	HOMO-1 → LUMO (96.8%)
	S ₀ → S ₅	2.3279	532.60	0.37490	HOMO-1 → LUMO+1 (50.8%) HOMO-2 → LUMO (48.3%)
	S ₀ → S ₆	2.3283	532.51	0.19940	HOMO-2 → LUMO+1 (96.8%)
	S ₀ → S ₈	2.6328	470.92	0.17580	HOMO-1 → LUMO+2 (99.5%)
	S ₀ → S ₉	2.6332	470.85	0.17560	HOMO-2 → LUMO+2 (99.5%)
	Transition	Energy (eV)	Wavelength (nm)	f	Electronic Configuration
[9]CMP	S ₀ → S ₁₂	4.9519	250.38	0.22360	HOMO-1 → LUMO+1 (28.6%) HOMO → LUMO+2 (28.6%) HOMO-2 → LUMO (22.8%) HOMO-8 → LUMO (6%)
	S ₀ → S ₂₁	5.1240	241.97	0.64180	HOMO-2 → LUMO+3 (31.6%) HOMO-2 → LUMO+1 (12.0%) HOMO-5 → LUMO+1 (6.7%) HOMO-4 → LUMO+2 (6.2%) HOMO → LUMO+2 (5.6%)
	S ₀ → S ₂₂	5.1243	241.95	0.65680	HOMO-2 → LUMO+4 (31.7%) HOMO-2 → LUMO+2 (11.9%) HOMO-5 → LUMO+2 (6.6%) HOMO-4 → LUMO+1 (6.5%) HOMO-1 → LUMO+2 (5.1%)
	S ₀ → S ₂₃	5.1527	241.09	1.15030	HOMO-3 → LUMO+4 (19.7%) HOMO-3 → LUMO+3 (14.7%) HOMO-1 → LUMO+5 (13.7%) HOMO-5 → LUMO (9.3%) HOMO-2 → LUMO+1 (5.4%)
	S ₀ → S ₂₄	5.1429	241.08	1.13560	HOMO-3 → LUMO+3 (19.9%) HOMO-3 → LUMO+4 (14.7%) HOMO → LUMO+5 (13.8%) HOMO-4 → LUMO (9.4%) HOMO-2 → LUMO+2 (5.6%)

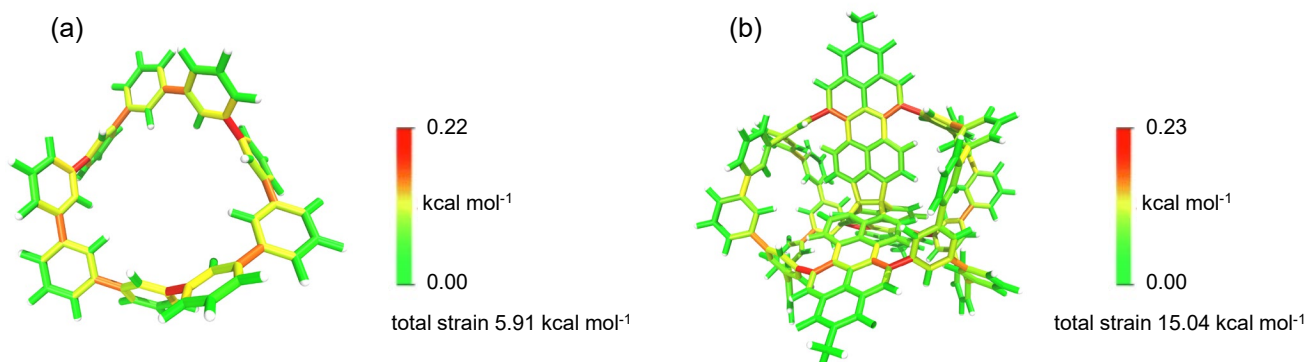


Fig. S11 StrainViz structures for [9]CMP and TPPTI-[9]CMP.

6. UV, CV and PL Spectra of Compounds

UV-vis absorption spectra were measured with Hitachi (model U-3010) and emission spectra were measured in CHCl_3 at room temperature; Fluorescence measurements were carried out on a FLS980 Spectrometer and quantum yield was determined by a Quanta- ϕ integrating sphere.

Cyclic voltammetry (CV) was recorded on a CHI620E electrochemical workstation using glassy carbon discs as the working electrode, Pt wire as the counter electrode, Ag/Ag^+ electrode as the reference electrode, and ferrocene/ferrocenium as an internal potential marker. The experiments were performed in nitrogen-purged DCM with tetrabutylammonium hexafluorophosphate (TBAPF_6 , 0.1 M) as the supporting electrolyte with a scan of 100 mV/s.

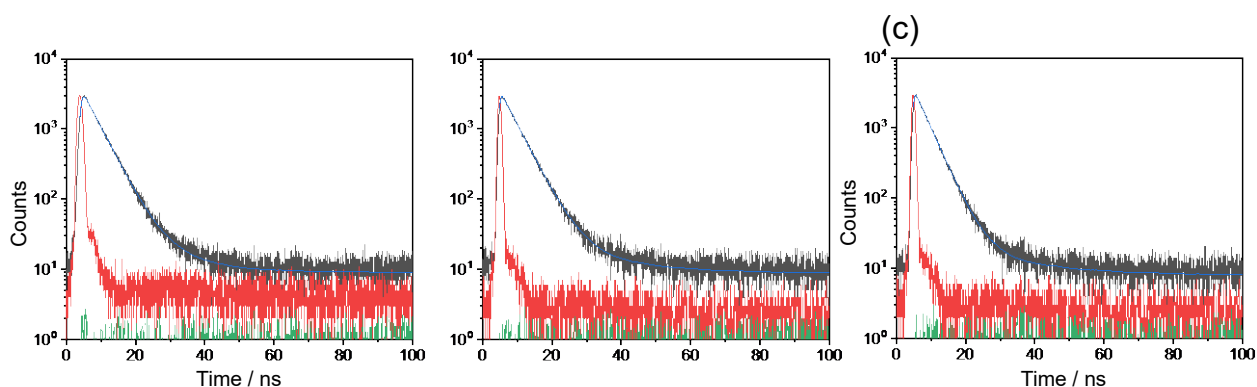


Fig. S12 Emission lifetime of [9]CMP (a), TPPTI-[9]CMP (b), and TPPTI (c) in chloroform.

7. Transient Absorption Measurements

Femtosecond transient absorption (fs-TA) measurements were performed by employing a Helios spectrometer (Ultrafast Systems LLC) equipped with a regenerative amplified Ti:sapphire laser system (coherent; 800 nm, 85 fs, 7 mJ pulse⁻¹, with 1 kHz repetition rate). The output pulse was split into two parts. One part was directed into a TOPAS optical parametric amplifier (OPA) to generate pump beam ranging from 250 nm to 2.5 μm . The other part of 800 nm beam was attenuated with a neutral density filter and focused into a 2 mm thick sapphire window to generate a white-light continuum (WLC) as probe beam. The pump-probe delay was controlled by a mechanical delay stage. Nanosecond transient absorption (ns-TA) measurements were conducted by using a commercial nanosecond transient spectrometer (Helios-EOS Fire, Ultrafast System Corporation).

All dilute solution samples were dissolved in a quartz cuvette (2 mm path length). Triplet photosensitization experiment was prepared by dissolving the sensitizer (anthracene, ~20 mM) and the sample (~20 μM) in CF. Anthracene could generate triplets by intersystem crossing and the energy could transfer to samples by diffusional collisions. All the samples prepared for ns-TA were preprocessed by degassing with N_2 for 10 min to eliminate the effect of O_2 on the triplets.

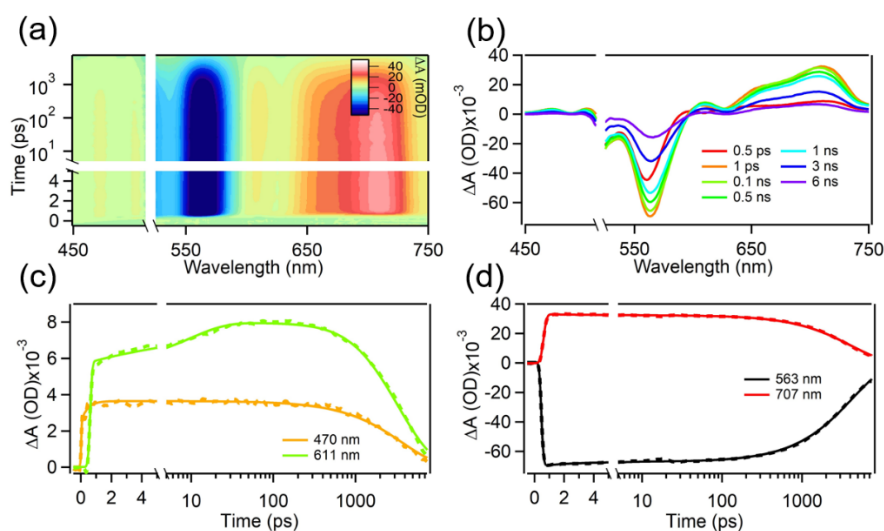


Fig. S13 (a) 2D contour map, (b) transient absorption spectra and (c, d) decay profiles of TPPTI-[9]CMP in dilute toluene solution with excitation at 520 nm.

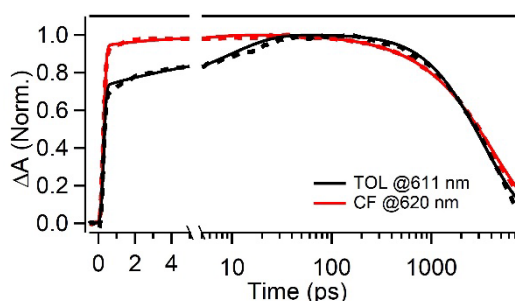


Fig. S14 The comparison of normalized decay profiles at corresponding wavelengths of TPPTI-[9]CMP in toluene (black) and chloroform (red).

In order to further clarify the assignment of the excited-state absorption (ESA) feature near 610 nm as charge-transfer (CT) state, we have compared the normalized decay profiles at corresponding wavelengths of TPPTI-[9]CMP in different solvents as shown in Fig. S13. It is shown that the rising process of ESA in CF ($\tau = 4.1$ ps) is faster than that in TOL ($\tau = 9.8$ ps), indicating that the formation of signal near 610 nm is polarity dependent. Therefore, ESA near 610 nm is mainly contributed from the charge transfer state.

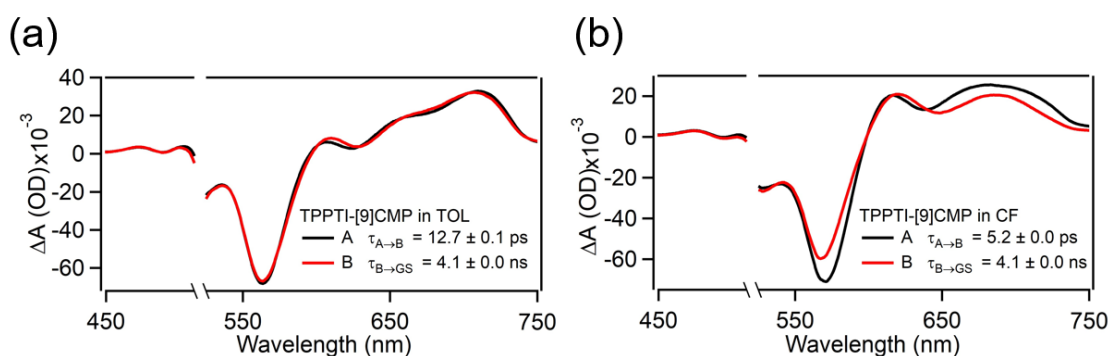


Fig. S15 The evolution-associated spectra (EAS) derived from global analysis results of fs-TA for TPPTI-[9]CMP in (a) toluene and (b) chloroform with corresponding time constants for specie evolution.

We have underwent global analysis for fs-TA with a sequential model to evaluate the dynamics and spectra shapes. As shown in Fig. S14a, there is a slight red shift for ESA band near 610 nm as specie A transfer to B within $\tau_{A \rightarrow B} = 12.7$ ps. Specie A represents the LE state while specie B is still dominated by LE state but with partial CT state.

In contrast, the band near 620 nm is much stronger in CF with higher polarity as shown in Fig. S14b. As band at 620 nm is dominated by CT state and 680 nm is assigned as LE state initially, the ratio of these two bands is reversed as specie A turning to B with a faster rate ($\tau_{A \rightarrow B} = 5.2$ ps). We assigned specie A as initial mixing state and B as CT state induced by polar solvent.

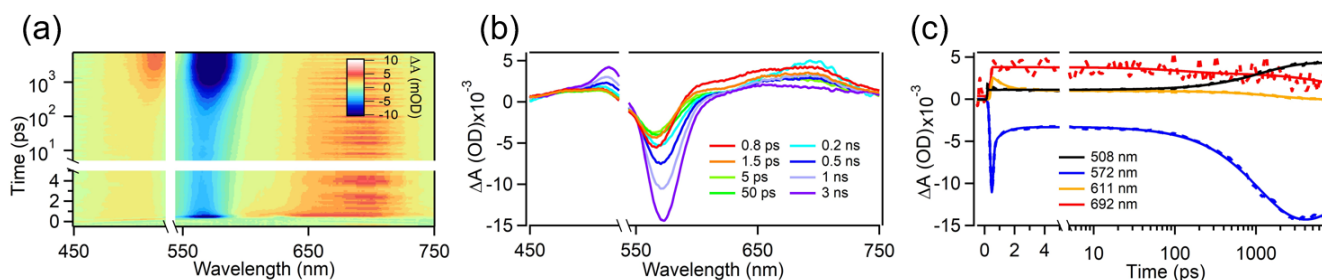


Fig. S16 (a) 2D contour map, (b) transient absorption spectra and (c) decay profiles of $(C_{60})_3@TPPTI-[9]CMP$ in dilute toluene solution with excitation at 530 nm.

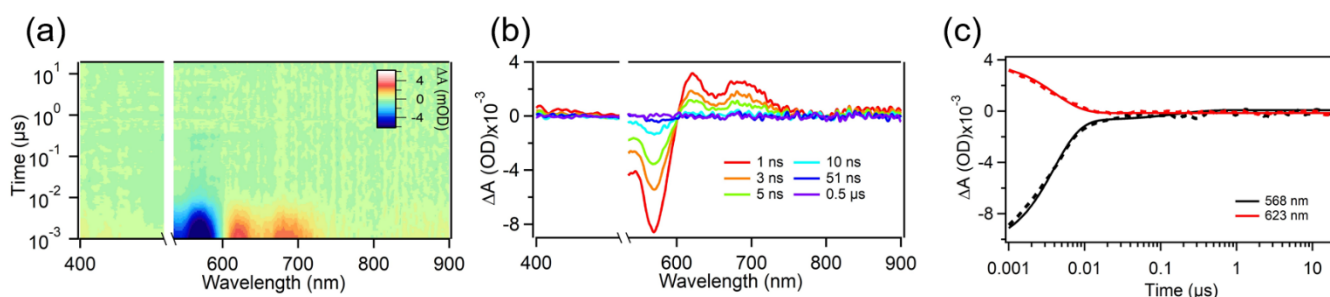


Fig. S17 ns-TA measurement for $TPPTI-[9]CMP$ in dilute chloroform with excitation at 520 nm: (a) 2D contour map, (b) transient absorption spectra and (c) decay profiles.

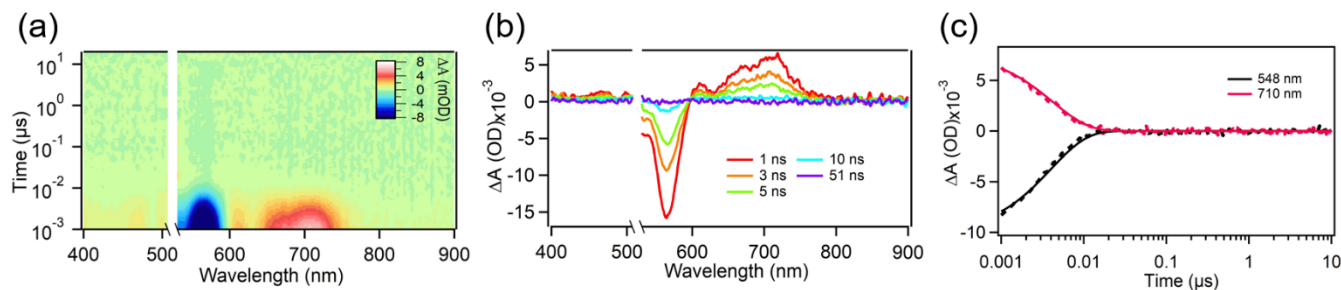


Fig. S18 ns-TA measurement for $TPPTI-[9]CMP$ in dilute toluene with excitation at 520 nm: (a) 2D contour map, (b) transient absorption spectra and (c) decay profiles.

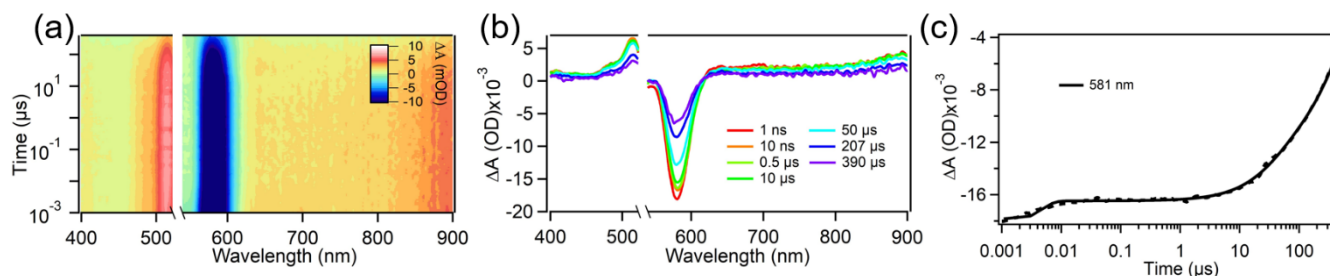


Fig. S19 ns-TA measurement for $(C_{60})_3@TPPTI-[9]CMP$ in dilute chloroform with excitation at 530 nm: (a) 2D contour map, (b) transient absorption spectra and (c) decay profiles.

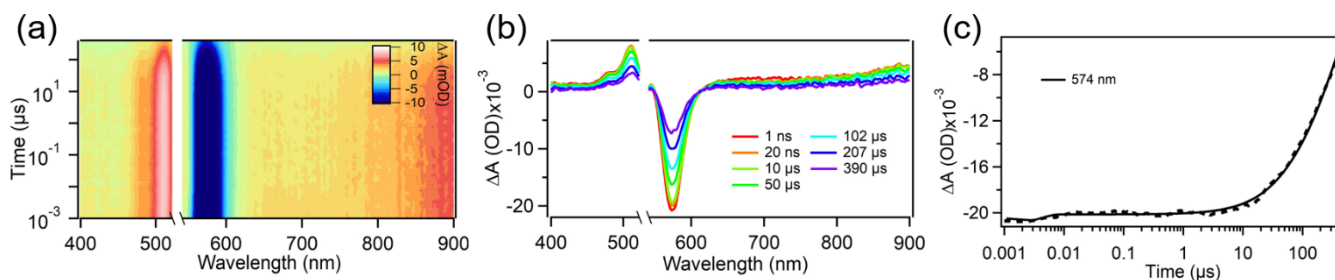


Fig. S20 Ns-TA measurement for $(C_{60})_3@TPPTI-[9]CMP$ in dilute toluene with excitation at 530 nm: (a) 2D contour map, (b) transient absorption spectra and (c) decay profiles.

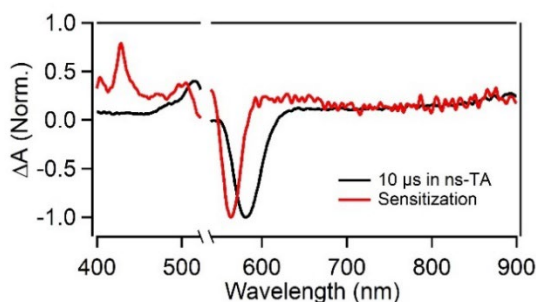


Fig. S21 The spectra of sensitized triplet for $TPPTI-[9]CMP$ (red) and the spectra of long-lived species (black) in $(C_{60})_3@TPPTI-[9]CMP$ are normalized and compare

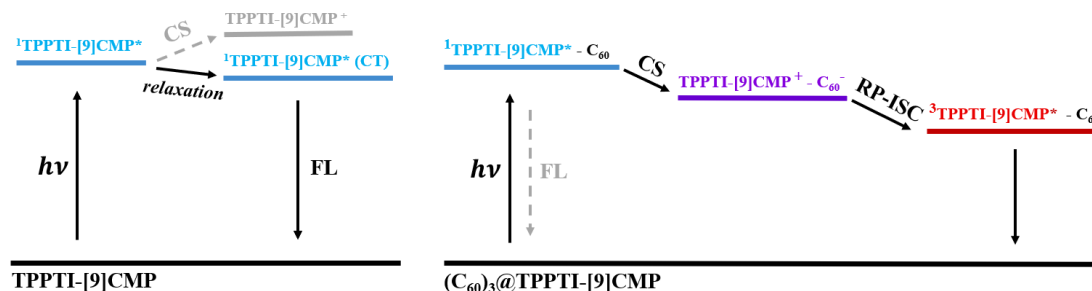


Fig. S22 Jablonski diagrams of excited state evolution in $TPPTI-[9]CMP$ and $(C_{60})_3@TPPTI-[9]CMP$.

8. Adsorption Isotherms Tests.

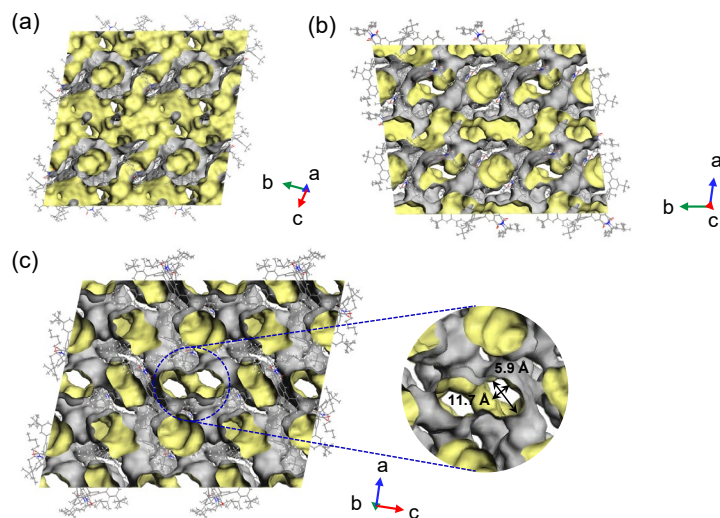


Fig. S23 Packing diagrams of $TPPTI-[9]CMP$ in different views: (a) a-axis and (b) c-axis, with the solvent-accessible void space visualized by yellow/grey (inner/outer) curved planes generated with a probe of 1.4 Å. (c) 3D packing

diagram and honeycomb-shaped channel of TPPTI-[9]CMP, The whole process is determined by single-crystal X-ray diffraction (SCXRD). Color code: gray, C; blue, N; red, O; white, H.

The adsorption and desorption isotherms of N₂ at 77 K, as well as the single-component gas adsorption isotherms of C₂H₄ and C₂H₆, were measured using the BSD 3H-2000 from Beishide Instrument Technology. Prior to testing, the samples were activated by vacuum heating at 100°C for 6 hours. The adsorption and desorption curves were then measured at 273 K, 283 K, and 298 K. After each set of isotherm measurements, the samples were re-activated through vacuum heating.

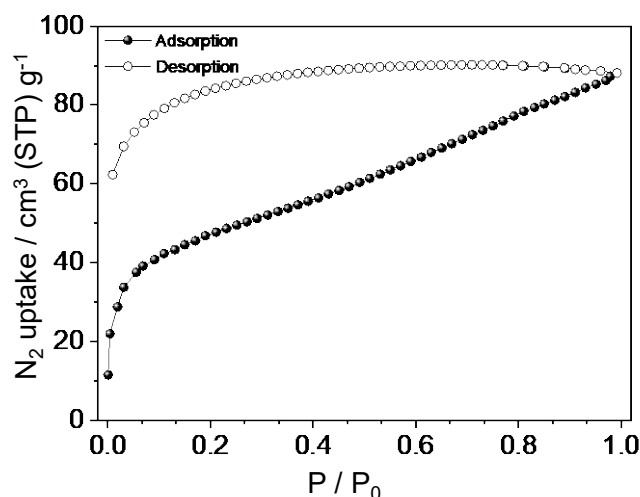


Fig. S24 N₂ adsorption-desorption Isotherm curves of TPPTI-[9]CMP at 77 K.

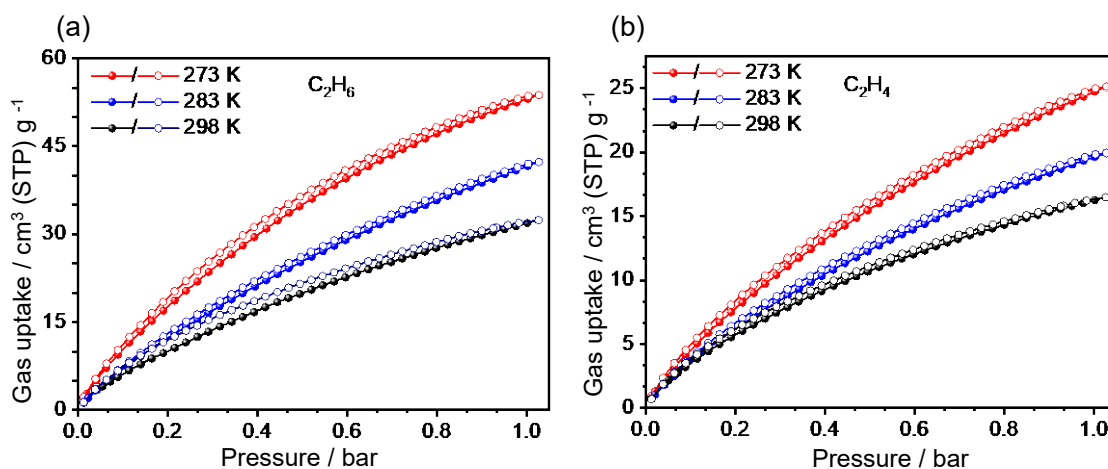


Fig. S25 Single-component adsorption isotherms of ethane (a) and ethylene (b) at 273 K, 283 K, and 298 K, respectively.

Table S3. Summary of adsorption quantity data at 1 bar at different temperatures

Gas uptake at 1bar (cm ³ g ⁻¹ STP)	C ₂ H ₆	C ₂ H ₄	C ₂ H ₆	C ₂ H ₄	C ₂ H ₆	C ₂ H ₄
Temperature	273 K		283 K		298 K	
TPPTI-[9]CMP	53.7241	25.13082	42.30074	19.93712	32.39995	16.47819

Table S4. Summary of the adsorption date of pure organic-based C₂H₆-selective adsorbents.

Adsorbents	C ₂ H ₆ uptake (mmol/g)	C ₂ H ₄ uptake (mmol/g)	Q _{st} (C ₂ H ₆ /C ₂ H ₄) (kJ/mol)	IAST Selectivity	Reference

TPPTI-[9]CMP	1.45	0.74	21.5/16.8	2.46	This work
7b	0.77	0.50	28.9/26.6	2.24	[9]
NKCOF-21	4.4	3.3	26.2/23.6	1.6	
NKCOF-22	2.9	1.8	25.9/24.1	1.5	[10]
NKCOF-23	2.7	2.2	24.3/23.0	1.3	
COF-1	2.4	1.9	22.5/22.2	1.92	
COF-6	2.1	2.1	29.2/27.5	1.20	
COF-8	1.6	1.5	27.5/25.1	1.21	
COF-10	1.0	0.9	26.6/25.1	1.31	[11]
MCOF-1	3.3	2.8	30.0/27.5	1.48	
COF-102	1.9	1.6	28.7/25.1	1.57	
COF-300	4.1	3.1	26.9/25.0	1.49	
COF-320	2.4	1.8	26.9/25.1	1.49	
CTF-DCTC-400	1.82	1.68	22.7/22.0	1.04	
CTF-DCTC-500	3.10	2.34	25.4/23.7	2.08	[12]
CTF-BT-500	4.5	3.9	24.1/23.3	1.3	[13]
DBA-3D-COF-1	2.09	1.7	16.8/15.9	1.24	[14]
HOF-BTB	3.09	2.49	25.4/22.6	1.4	[15]
ZJU-HOF-1	4.87	3.87	31.5/-	2.25	[16]
HOF-76a	2.95	1.67	22.8/20.6	2.05	[17]

9. Breakthrough Curves Tests.

The dynamic penetration experiment for C_2H_6 and C_2H_4 was conducted using the BSD-MAB instrument. A 480 mg sample, which had been vacuumed and heated at $100^\circ C$ for 2 hours, was placed into an adsorption column (Φ_{10} mm diameter \times 100 mm length) and purged with inert gas for two hours. The dynamic penetration test was carried out at 1 bar and 298 K. During the experiment, the C_2H_6/C_2H_4 ratio was 1:1, with a total gas flow rate of 5 mL/min.

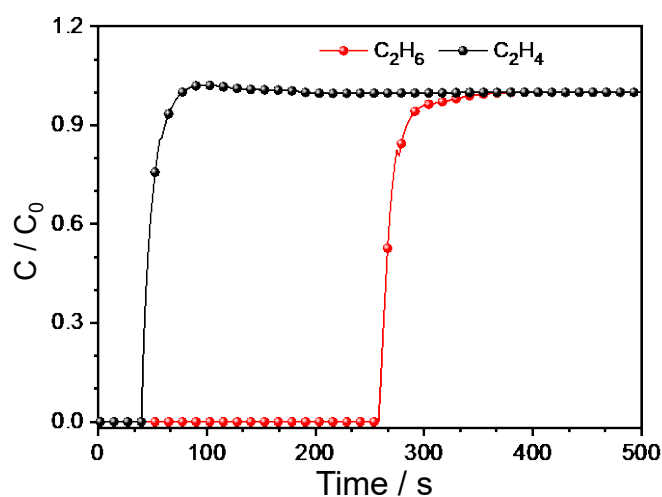


Fig. S26 The experimental breakthrough curve of TPPTI-[9]CMP for C_2H_6/C_2H_4 (1/1, v/v, no carrier gas) at 298 K and 1 bar with a total flow rate was 5 mL min^{-1} .

10. IAST (Ideal adsorbed solution theory) Selectivity Calculations.

IAST (Ideal adsorbed solution theory)^[18] was used to predict binary mixture adsorption from the pure gas isotherms. The experimental adsorption isotherm data for C_2H_4 and C_2H_6 at 298 K were fitted with a dual Langmuir-Freundlich (L-F) model:

$$(1) q = \frac{a_1 * b_1 * P^{c_1}}{1 + b_1 * P^{c_1}} + \frac{a_2 * b_2 * P^{c_2}}{1 + b_2 * P^{c_2}}$$

Where q is the adsorption amounts and P is the pressure, respectively.

The adsorption selectivity for binary mixtures defined by

$$(2) S_{A/B} = \frac{x_A y_B}{x_B y_A}$$

were respectively calculated using the Ideal Adsorption Solution Theory (IAST). Where x_A is the mole fraction of component A in the adsorbed phase and y_A is the mole fraction of component A in the bulk.

11. Isothermic Heats of Adsorption (Q_{st}) Calculations.

The isosteric heats of adsorption (Q_{st}) was calculated by the Virial equation^[19], which is as follows:

$$(3) \ln P = \ln N + \frac{1}{T} \sum_{i=0}^m a_i N^i + \sum_{i=0}^n b_i N^i$$

$$(4) Q_{st} = -R \sum_{i=0}^m a_i N^i$$

Where P is the pressure, N is the adsorption capacity (mmol/g), T is the temperature, a_i and b_i are parameters independent of temperature, m , n are the number of a_i and b_i respectively, R is the universal gas constant.

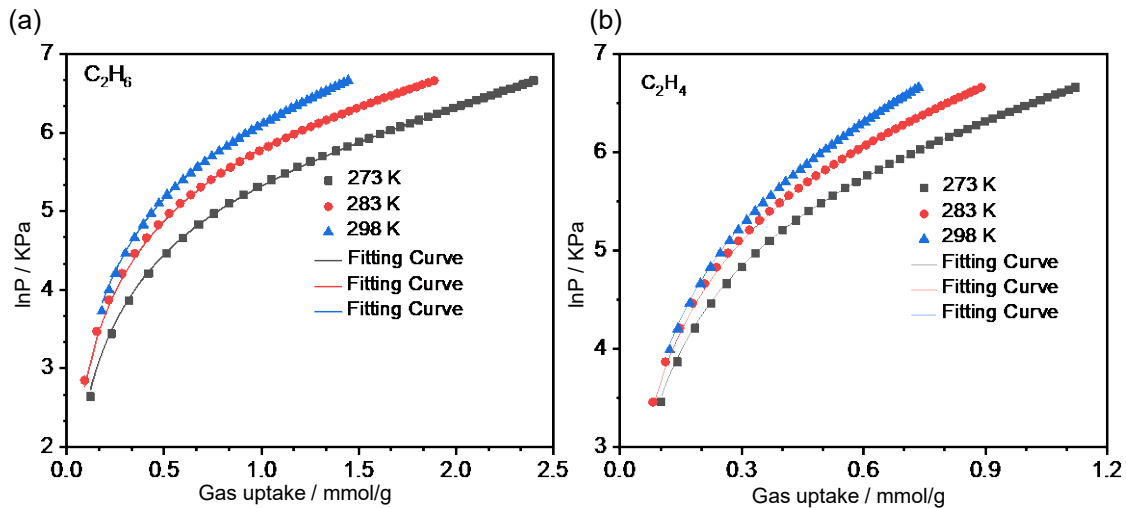


Fig. S27 Virial equation fitting of C_2H_6 (a) and C_2H_4 (b) adsorption isotherms.

Table S5. The fitting parameters of Virial equation at isosteric enthalpies of adsorption.

Parameter	C_2H_6	C_2H_4
a_0	-1912.58593	-768.40077
a_1	-882.72098	-2038.22077
a_2	-33.4778	-468.01631
a_3	381.10633	2382.05179
a_4	-132.43294	-1689.54062
a_5	18.21951	481.41195
b_0	11.66953	8.37679
b_1	4.88297	10.32455
b_2	-1.84769	-4.53732
Adj.R-square	0.99964	0.99973

12. Binding Energy Calculations.

Periodic DFT calculations were performed to optimize the host-guest system and binding energy of C_2H_6/C_2H_4 interaction with the molecule of x, using Perdew-Burke-Ernzerhof (PBE) method^[20,21] with Grimme's DFT-D correction^[22] in Dmol₃^[23] module in Materials Studio 8.0 of Accelrys.^[22-26]

The tolerances of energy, gradient and displacement convergence were, 1×10^{-5} hartree, 2×10^{-3} hartree \AA^{-1} , and 5×10^{-3} \AA , respectively.

The binding energy (ΔE_{bind}) for C_2H_6/C_2H_4 with models was calculated by Supplementary Equation X,

$$\Delta E_{\text{bind}} = E_{AB} - E_A - E_B \quad (X)$$

where, E_{AB} , E_A , and E_B are the total energies of complex of gas with model, single C_2H_6/C_2H_4 gas, and TPPTI-[9]CMP model at the optimized geometries, respectively.

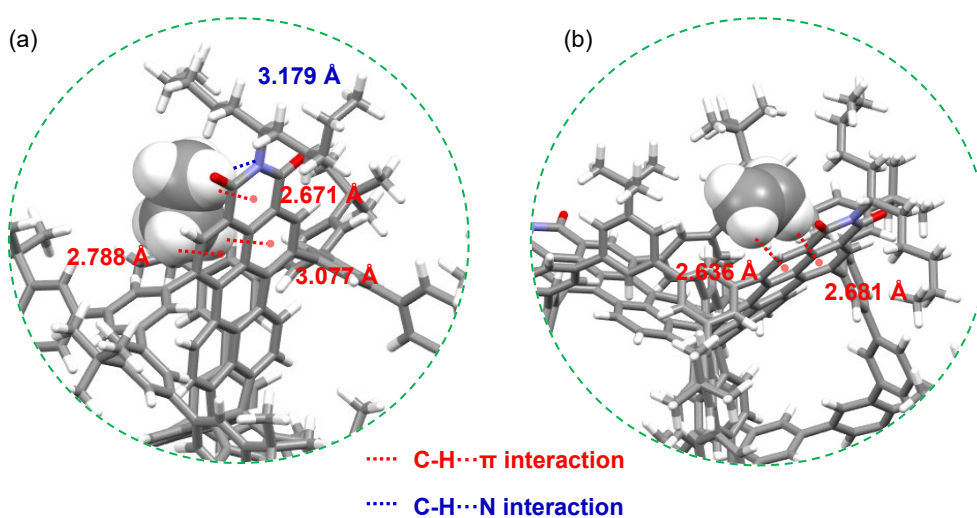


Fig. S28 The calculated CH... π interactions, CH...N bond, and adsorption sites in TPPTI-[9]CMP for C_2H_6 (a) and C_2H_4 (b).

13. ¹H NMR, ¹³C NMR, and HRMS Spectra of Compounds

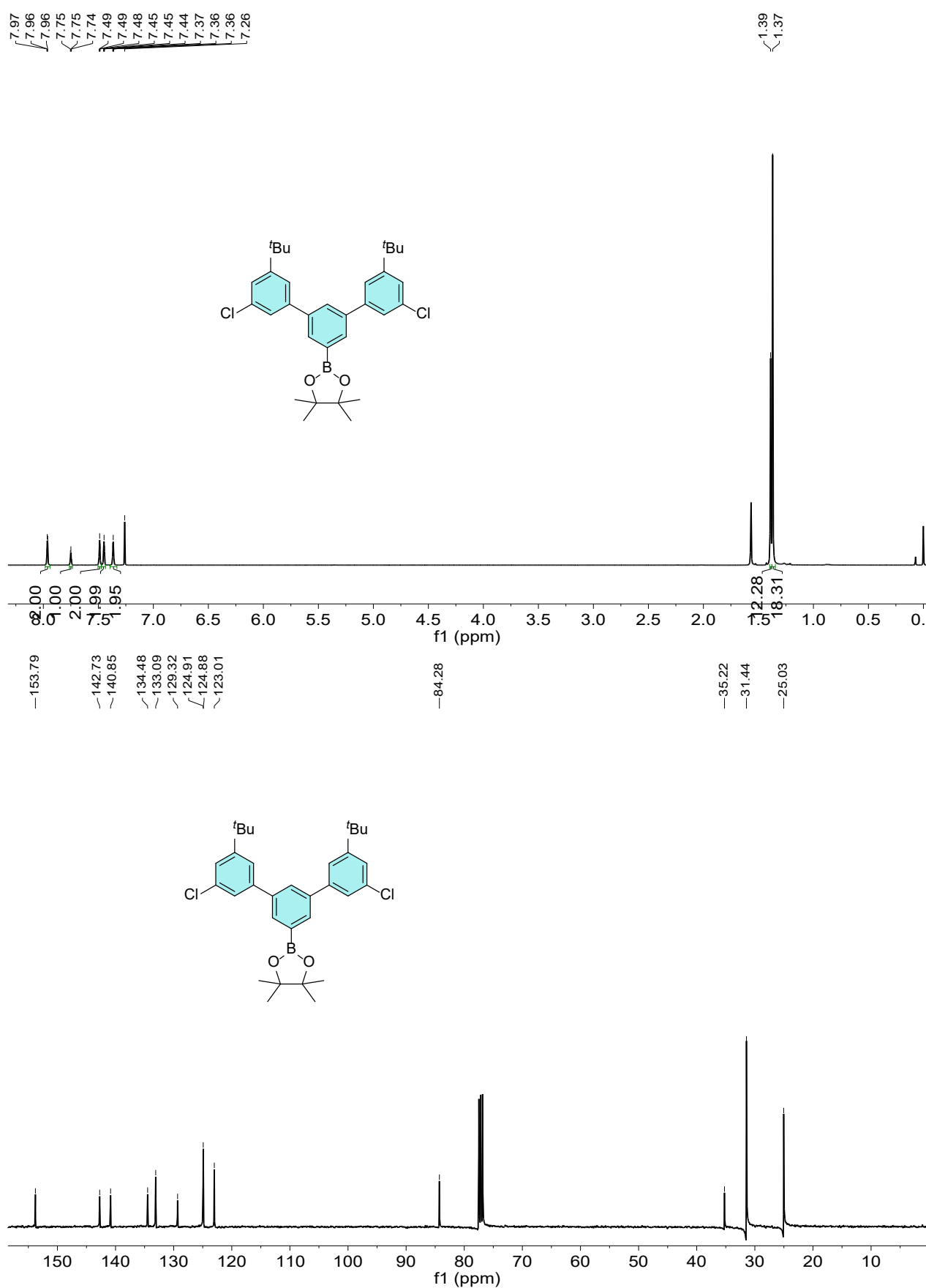


Fig. S29 ¹H NMR and ¹³C NMR spectra of *m*-terphenyl borate **2** in CDCl₃ (400 MHz, 298 K).

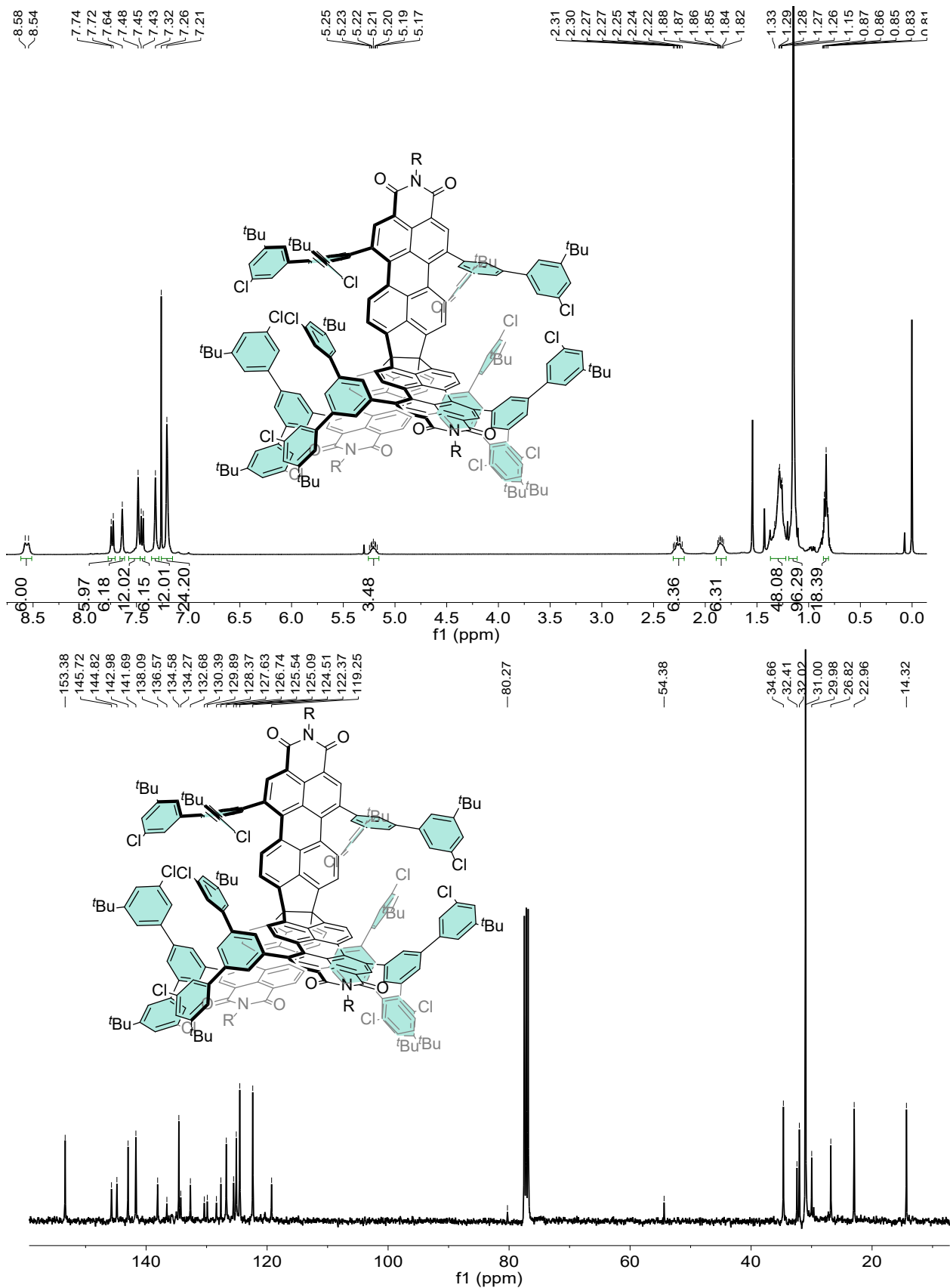


Fig. S30 ^1H NMR spectrum of compound **3** in CDCl_3 (400 MHz, 298 K) and ^{13}C NMR spectrum of compound **3** in $\text{CDCl}_3/\text{CS}_2$ (400 MHz, 298 K).

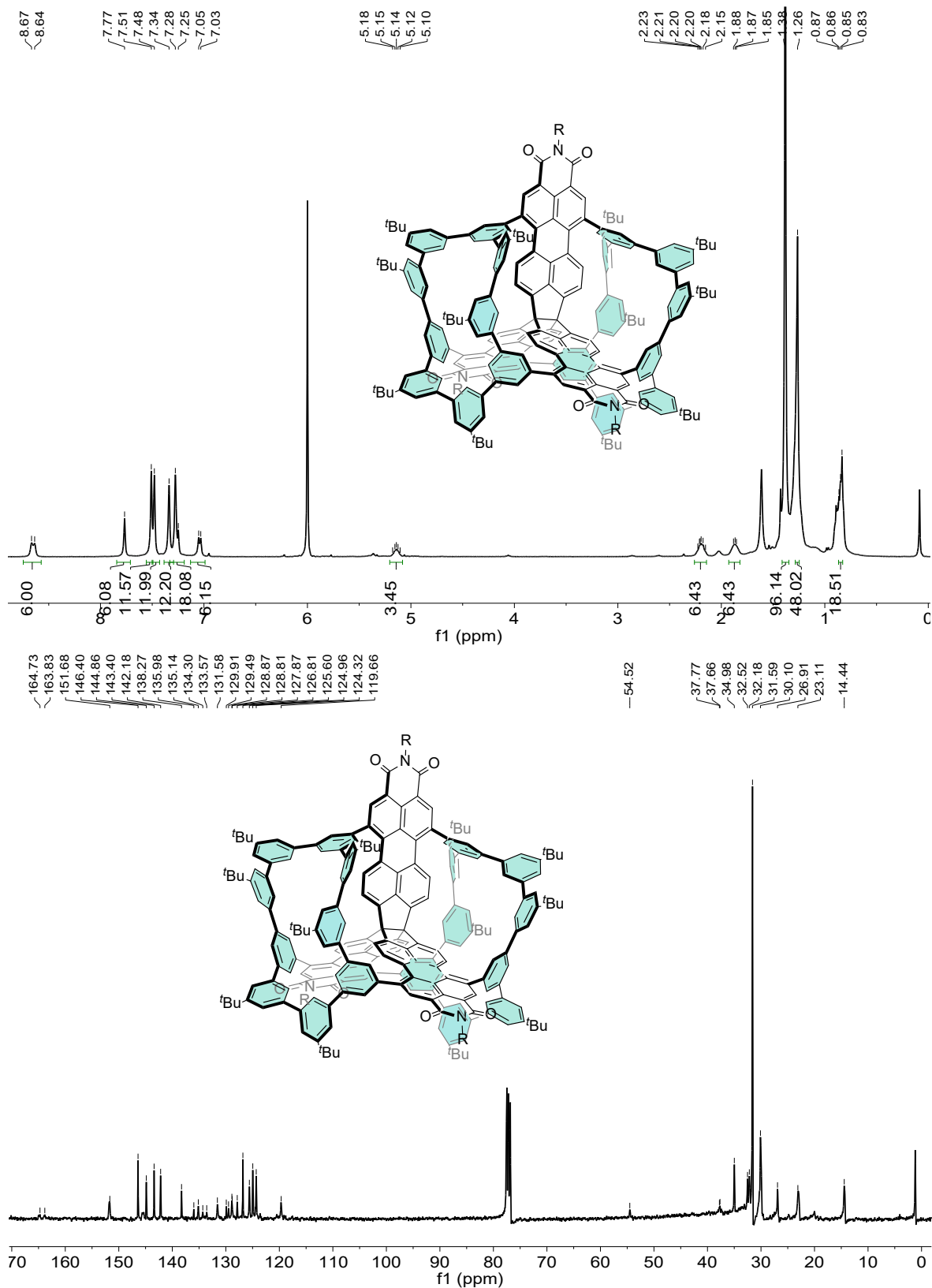


Fig. S31 ¹H NMR spectrum of TPPTI-[9]CMP in C₂D₂Cl₄ (400 MHz, 298 K) and ¹³C NMR spectrum of TPPTI-[9]CMP in CDCl₃/CS₂ (400 MHz, 298 K).

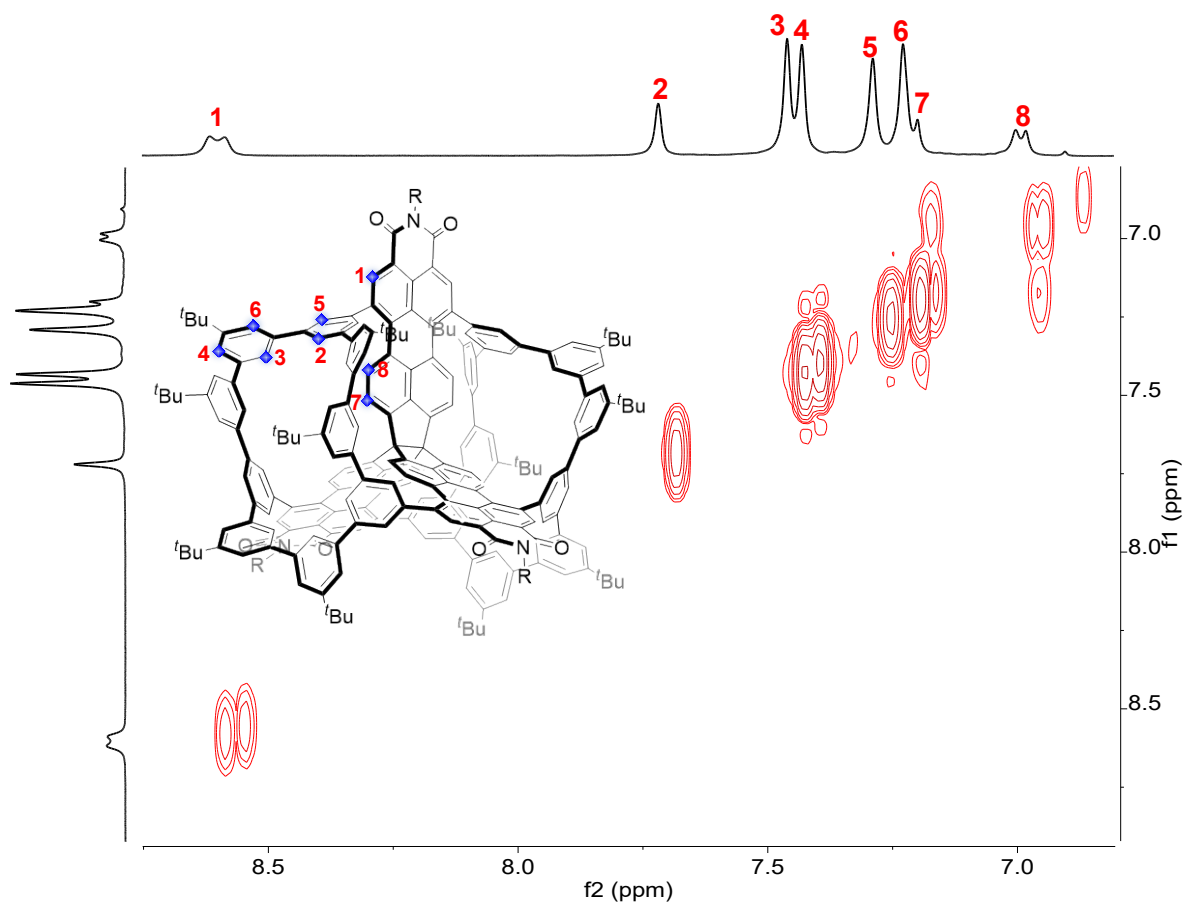


Fig. S32 ^1H COSY NMR spectrum of TPPTI-[9]CMP (600 MHz, $\text{C}_2\text{D}_2\text{Cl}_4$, 298 K).

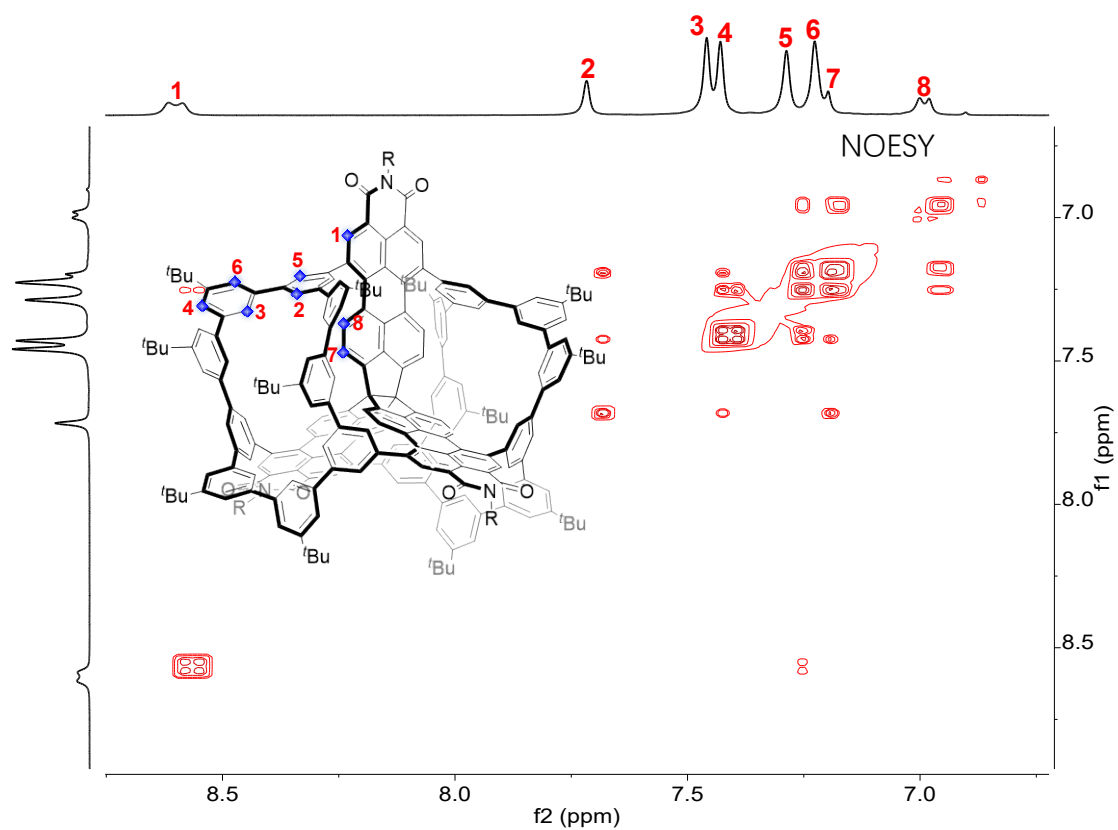


Fig. S33 ^1H NOESY NMR spectrum of TPPTI-[9]CMP (600 MHz, $\text{C}_2\text{D}_2\text{Cl}_4$, 298 K).

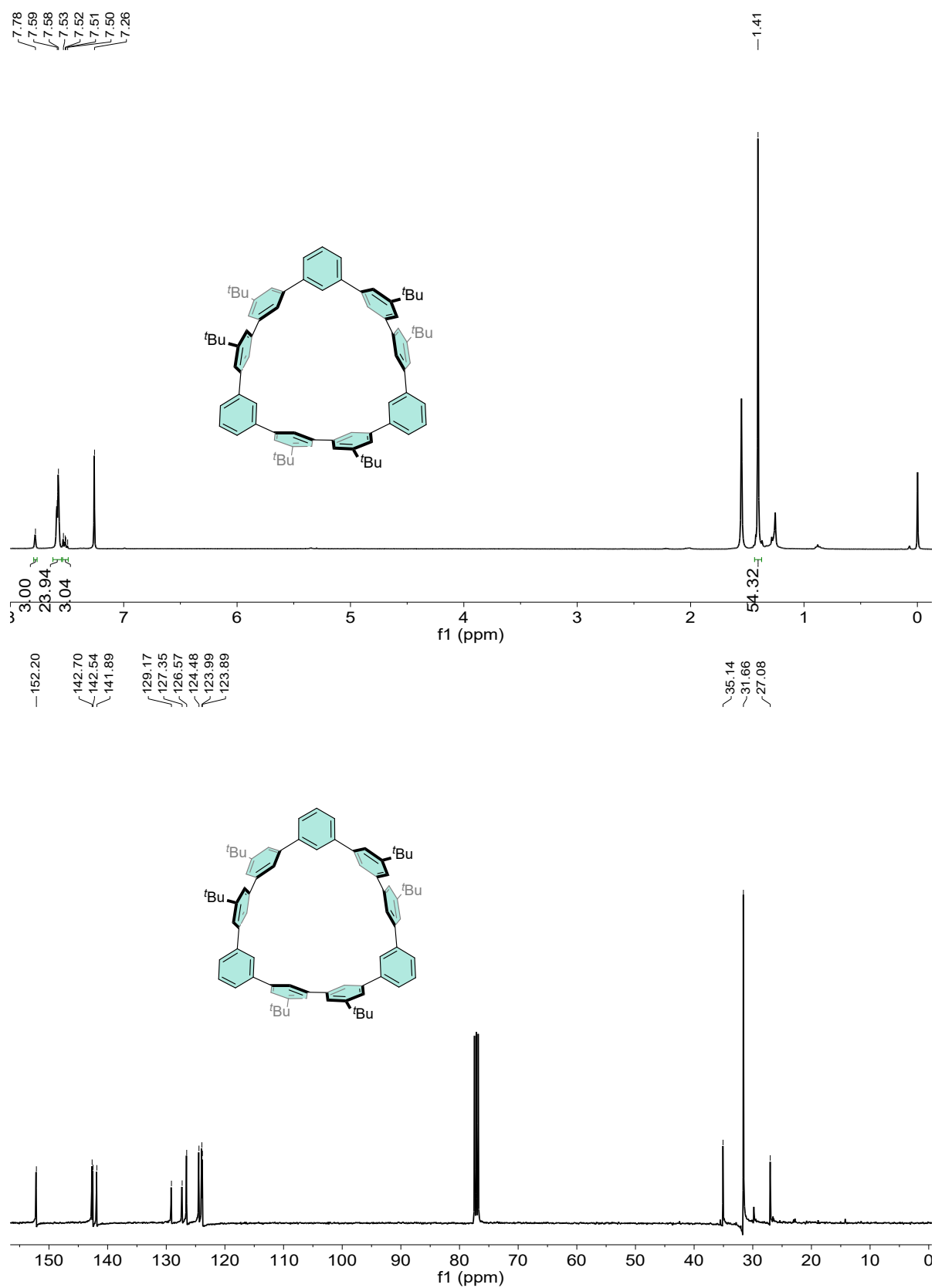


Fig. S34 ¹H NMR and ¹³C NMR spectra of [9]CMP in CDCl₃ (400 MHz, 298 K).

Acquisition Parameter

Acquisition Mode	Single MS	Acquired Scans	2	Calibration Date	Wed Sep 25 05:23:00
Polarity	Positive	No. of Cell Fills	1	Data Acquisition Size	2097152
Broadband Low Mass	202.1 m/z	No. of Laser Shots	20	Data Processing Size	4194304
Broadband High Mass	2000.0 m/z	Laser Power	39.8 lp	Apodization	Sine-Bell Multiplication
Source Accumulation	0.001 sec	Laser Shot Frequency	0.020 sec		
Ion Accumulation Time	0.010 sec				

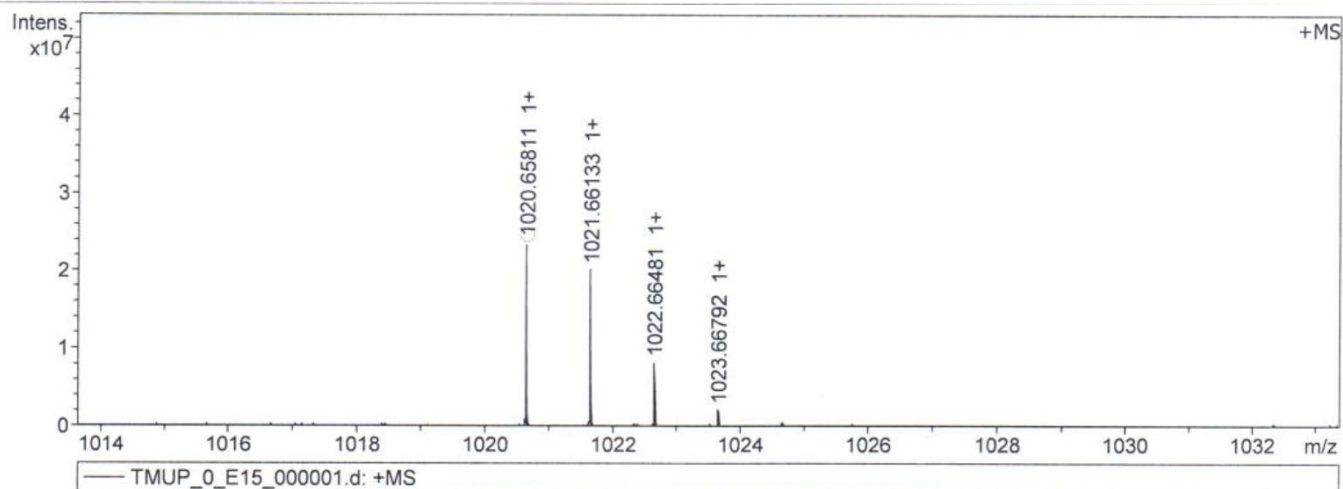


Fig. S35 HR-MALDI-TOF Spectrum of [9]CMP.

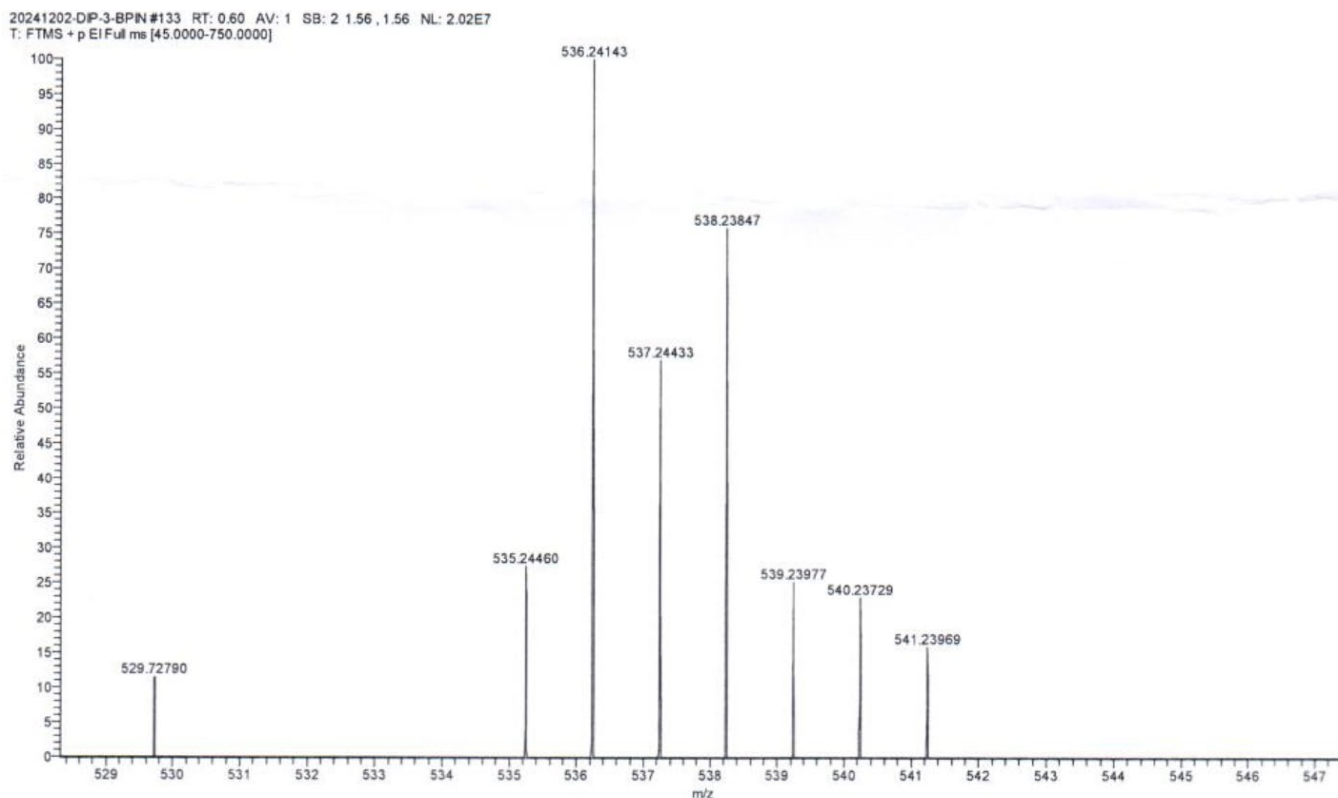
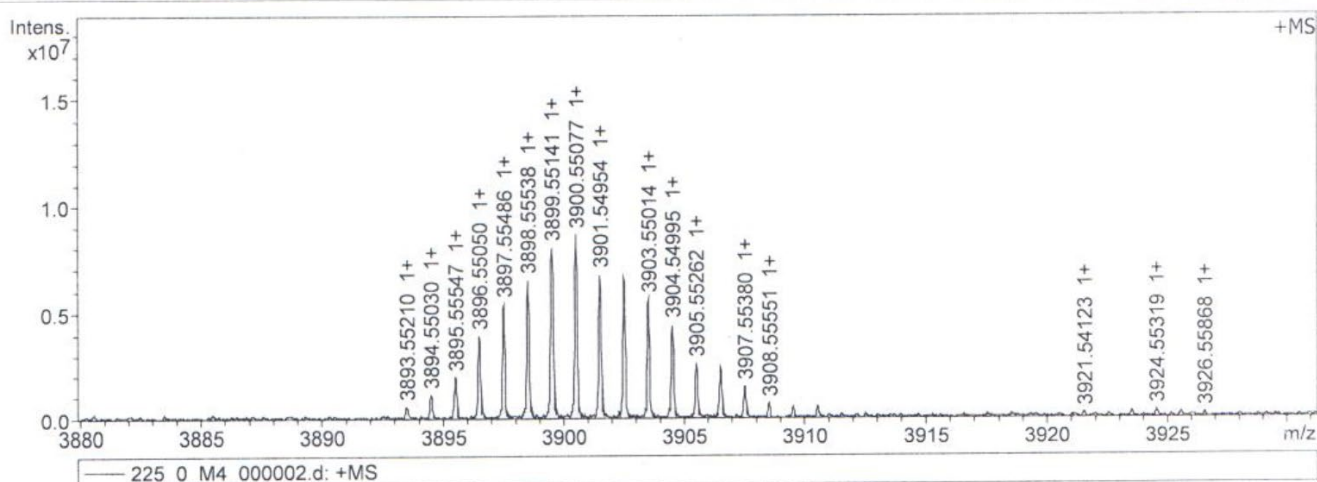


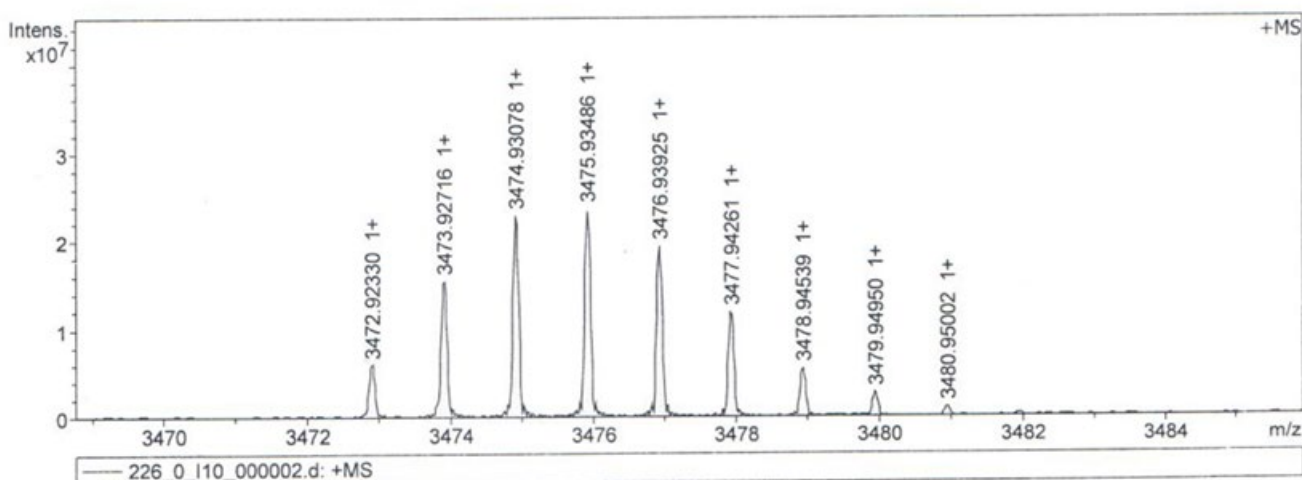
Fig. S36 HR-EI-MS Spectrum of *m*-terphenyl borate 2.

Acquisition Parameter

Acquisition Mode	Single MS	Acquired Scans	1	Calibration Date	Thu Oct 31 03:34:59
Polarity	Positive	No. of Cell Fills	1	Data Acquisition Size	2097152
Broadband Low Mass	202.1 m/z	No. of Laser Shots	66	Data Processing Size	4194304
Broadband High Mass	7500.0 m/z	Laser Power	41.0 lp	Apodization	Sine-Bell Multiplication
Source Accumulation	0.001 sec	Laser Shot Frequency	0.020 sec		
Ion Accumulation Time	0.010 sec				

**Fig. S37** HR-MALDI-TOF Spectrum of compound **3**.**Acquisition Parameter**

Acquisition Mode	Single MS	Acquired Scans	2	Calibration Date	Mon Mar 11 04:33:04
Polarity	Positive	No. of Cell Fills	1	Data Acquisition Size	2097152
Broadband Low Mass	202.1 m/z	No. of Laser Shots	57	Data Processing Size	4194304
Broadband High Mass	6800.0 m/z	Laser Power	50.2 lp	Apodization	Sine-Bell Multiplication
Source Accumulation	0.001 sec	Laser Shot Frequency	0.020 sec		
Ion Accumulation Time	0.010 sec				

**Fig. S38** HR-MALDI-TOF Spectrum of TPPTI-[9]CMP.

14. References

- [1] K. Ikemoto, R. Kobayashi, S. Sato and H. Isobe. *Angew. Chem. Int. Ed.* 2017, **56**, 6511.
- [2] Z. Sun, T. Mio, K. Ikemoto, S. Sato and H. Isobe. *J. Org. Chem.* 2019, **84**, 3500.
- [3] A. L. Spek, *Acta Crystallogr.* 2015, **C71**, 9.
- [4] Gaussian 09, Revision D.01, M. J. Frisch, G. W. Trucks, H. B. Schlegel, G. E. Scuseria, M. A. Robb, J. R. Cheeseman, G. Scalmani, V. Barone, B. Mennucci, G. A. Petersson, H. Nakatsuji, M. Caricato, X. Li, H. P. Hratchian, A. F. Izmaylov, J. Bloino, G. Zheng, J. L. Sonnenberg, M. Hada, M. Ehara, K. Toyota, R. Fukuda, J. Hasegawa, M. Ishida, T. Nakajima, Y. Honda, O. Kitao, H. Nakai, T. Vreven, J. A. Montgomery, Jr., J. E. Peralta, F. Ogliaro, M. Bearpark, J. J. Heyd, E. Brothers, K. N. Kudin, V. N. Staroverov, T. Keith, R. Kobayashi, J. Normand, K. Raghavachari, A. Rendell, J. C. Burant, S. S. Iyengar, J. Tomasi, M. Cossi, N. Rega, J. M. Millam, M. Klene, J. E. Knox, J. B. Cross, V. Bakken, C. Adamo, J. Jaramillo, R. Gomperts, R. E. Stratmann, O. Yazyev, A. J. Austin, R. Cammi, C. Pomelli, J. W. Ochterski, R. L. Martin, K. Morokuma, V. G. Zakrzewski, G. A. Voth, P. Salvador, J. J. Dannenberg, S. Dapprich, A. D. Daniels, O. Farkas, J. B. Foresman, J. V. Ortiz, J. Cioslowski, and D. J. Fox, Gaussian, Inc., Wallingford CT, 2013.
- [5] T. Lu., and F. Chen., Multiwfn: A Multifunctional Wavefunction Analyzer, *J. Comput. Chem.* 2012, **33**, 580
- [6] T. Lu, and Q. Chen, *J. Comput. Chem.* 2022, **43**, 539.
- [7] W. Humphrey, A. Dalke and K. Schulten, *J. Mol. Graph.* 1996, **14**, 33.
- [8] C. E. Colwell, T. W. Price, T. Stauch and R. Jasti, *Chem. Sci.*, 2020, **11**, 3923.
- [9] Y. Chen, Y. Zhao, Y. Zhao, X. Chen, X. Liu, L. Li, D. Cao, S. Wang and L. Zhang, *Angew. Chem. Int. Ed.* 2024, e202401706.
- [10] F. Jin, E. Lin, T. Wang, S. Geng, T. Wang, W. Liu, F. Xiong, Z. Wang, Y. Chen, P. Cheng and Z. Zhang, *J. Am. Chem. Soc.* 2022, **144**, 5643.
- [11] C. He, Y. Wang, Y. Chen, X. Wang, J. Yang, L. Li and J. Li, *ACS Appl. Mater. Interfaces* 2020, **12**, 52819.
- [12] Y. Chang, H. Huang, H. Zhu, Y. Zhao, L. Wang, Y. Sun and C. Zhong, *Chem. Eng. J* 2022, 427.
- [13] J. Wang, X. Lian, Z. Zhang, X. Liu, Q. Zhao, J. Xu, X. Cao, B. Li and X. H. Bu, *Chem. Commun.* 2023, **59**, 11240.
- [14] L. A. Baldwin, J. W. Crowe, D. A. Pyles and P. L. McGrier, *J. Am. Chem. Soc.* 2016, **138**, 15134.
- [15] T. U. Yoon, S. B. Baek, D. Kim, E. J. Kim, W. G. Lee, B. K. Singh, M. S. Lah, Y. S. Bae and K. S. Kim, *Chem. Commun.* 2018, **54**, 9360.
- [16] X. Zhang, J. X. Wang, L. Li, J. Pei, R. Krishna, H. Wu, W. Zhou, G. Qian, B. Chen and B. Li, *Angew. Chem. Int. Ed.* 2021, **60**, 10304.
- [17] X. Zhang, L. Li, J. X. Wang, H. M. Wen, R. Krishna, H. Wu, W. Zhou, Z. N. Chen, B. Li, G. Qian and B. Chen, *J. Am. Chem. Soc.* 2020, **142**, 633.
- [18] G. D. Wang, R. Krishna, Y. Z. Li, W. J. Shi, L. Hou, Y. Y. Wang and Z. Zhu, *Angew. Chem. Int. Ed.* 2022, **61**, e202213015.
- [19] L. Li, R. Krishna, H. Li, S. Xiang, H. Wu, J. Li, W. Zhou and B. Chen, *Science* 2018, **362**, 443.
- [20] J. P. Perdew, K. Burke and M. Ernzerhof, *Phys. Rev. Lett.* 1996, **77**, 3865.
- [21] S. Grimme, S. Ehrlich and L. Goerigk, *J. Comput. Chem.* 2011, **32**, 1456.
- [22] S. Grimme, J. Antony, S. Ehrlich and H. Krieg, *J. Chem. Phys.* 2010, **132**, 154104.
- [23] B. Delley, *J. Chem. Phys.* 2000, **113**, 7756.

[24] Material Studio. Versiono 8.0 edn. 2014, Accelrys Inc.

[25] M. P. Allen and D. J. Tildesley, Computer simulation of liquids. Oxford university, 2017.

[26] D. Frenkel and B. Smit, Understanding molecular simulation: from algorithms to applications. Elsevier, 2023.